Corrosion Resistance of NZP and Aluminum Titanate

by

Yangsheng Lu

Thesis submitted to the Faculty of the

Virginia Polytechnic Institute and State University

in partial fulfillment of the requirements for the degree of

Master of Science

in

Materials Science and Engineering

Approved:

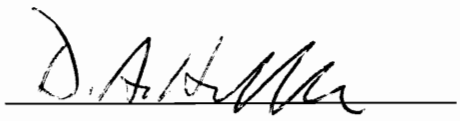

D. A. Hirschfeld

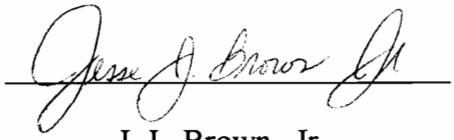

J. J. Brown, Jr.

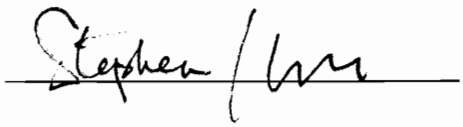

S. L. Kampe

September, 1996

Blacksburg, Virginia

Corrosion Resistance of NZP and Aluminum Titanate

by

Yangsheng Lu

D. A. Hirschfeld, Chairperson

Department of Materials Science and Engineering

(Abstract)

To determine the feasibility of using low thermal expansion ceramics and aluminum titanate in diesel engine applications, the mechanical and thermal properties and corrosion resistance were evaluated. NZP ($Ba_{1.25}Zr_4P_{5.5}Si_{0.5}O_{24}$ and $Ca_{0.5}Sr_{0.5}Zr_4P_6O_{24}$) and aluminum titanate (AT) were exposed to a simulated diesel engine environment.

The effects of thermal cycling from room temperature to 700°C, and a combination of alkali corrosion and thermal cycling on the mechanical and thermal properties of these ceramics were examined. It was found that NZP and AT materials demonstrated near zero bulk thermal expansion, good thermal up shock resistance and resistance to Na and V corrosion, because of their porous structure and low density. However, the AT materials exhibited lower flexural strength. This is a direct result of the inherent microcracking across the AT grains upon cooling from the sintering temperature, which reduces the flexural strength and elastic modulus.

Acknowledgements

The author would like to express her gratitude to the members of her committee, Dr. D.A. Hirschfeld, Dr. J.J. Brown, Jr., and Dr. S.L. Kampe. To Dr. Hirschfeld, committee chair, for her constant support, patience, and encouragement throughout this work. To Dr. Brown for his offer of a Research Associate position in the Center for Advanced Ceramic Materials. Without his recommendation, I would not have had the chance to continue my professional career in ceramic engineering. To Dr. Kampe for his valuable discussions and insightful lectures.

Several professors in the Department of Materials Science and Engineering and the Center for Advanced Ceramic Materials have made my study and research very challenging and rewarding. They are Drs. G.V. Gibbs, D.P.H. Hasselman, and R.G. Kander. I would like to extend my appreciation to them.

Administrative staff in the Center for Advanced Ceramic Materials and the Department of Materials Science and Engineering and my fellow graduates have made my stay at Virginia Tech very memorable. They are LeeAnn Ellis, Jan Doran, Amy Hill, Susan Fleming, and Bill Russ.

Love from my family, my husband Zhaoyang, my lovely daughter Sherry, and my always smiling sons Peter and Andrew, has been essential for me to carry out this project.

Table of Contents

List of Figures

List of Tables

Chapter 1. Introduction

Ceramic materials with low coefficients of thermal expansion (CTE) offer several benefits, including superior thermal shock resistance, the ability to maintain dimensional stability over large temperature ranges, and the ability to withstand large thermal gradients. These properties make them desirable for diesel engine applications such as exhaust particulate traps, catalyst substrates, exhaust port liners, and piston crown insulation. One application, "cast-in-place" exhaust port liners, is the focus of this study.

Ceramics used in making exhaust port liners must exhibit properties that enable them to survive harsh environments and thermal cycling requirements needed to lengthen the operating life of the part. Low thermal expansion is required to prevent the failure of the exhaust port liner due to thermal shock during the molten metal casting process. The ceramic must also exhibit high corrosion resistance and thermal cycling resistance to be suitable for an engine operating environment [1-7] since the effects of corrosion are enhanced with higher operating temperatures. Impurities in fuel such as sodium carbonate and vanadia are the main corrosive agents encountered in this application.

NZP ($Ba_{1.25}Zr_4P_{5.5}Si_{0.5}O_{24}$ and $Ca_{0.5}Sr_{0.5}Zr_4P_6O_{24}$) developed by LoTEC, Inc., and aluminum titanate (AT-80), developed by Golden Technologies Company (GTC), were the low expansion ceramics selected for this study. For the application of "cast-in-place" exhaust port liners, the effect of thermal up shock, corrosion, and thermal cycling on

thermal and mechanical properties of these materials must be evaluated, which is the goal of this study.

The corrosion resistance of NZP and aluminum titanate was evaluated by coating samples with sodium, vanadium, and combined sodium/vanadium solutions, then cycling from room temperature to 700°C to determine the effect of corrosion/thermal cycling. The corrosion resistance was characterized by dilatometry, environmental scanning electron microscopy (ESEM), variations in weight gain, and changes in mechanical properties.

Chapter 2. Literature Review

2.1 NZP Ceramics

2.1.1 Thermal Expansion Behavior

NZP ceramics (sodium zirconium phosphate and its crystal structure analog) are a relatively new class of low to ultra-low thermal expansion materials. The thermal expansion behavior of NZP ceramics can be explained in terms of a structural model based on rotation of the polyhedral network of the lattice [8,9]. The crystal structure of NZP is a hexagonal structure with $R\bar{3}C$ space asymmetry, as schematically shown in Figure 2.1 [9], and is built up of PO_4 tetrahedra and ZrO_6 octahedral which are linked on corners to form a three-dimensional network. The bonds are strong and the skeletons are stable. These bonds can bend and result in a small rotation without breaking the structure. The interstitial sites M' and M", which are the holes or vacancies in the skeleton, can be left vacant without changing the crystal structure and allow a variety of ionic substitutions [10, 11]; for example, Ca^{2+} ions are substituted by Mg^{2+} ions forming a $(Ca_{1-x}Mg_x)Zr(PO_4)_6$ (CMZP) crystal structure.

The framework structure of NZP, Figure 2.1, expands in the **c**-axis direction when heated while the PO_4 groups rotate; at the same time, the structure contracts in the *a*-axis direction [9]. In contrast, the PO_4 groups can rotate in the opposite direction, which results in an expansion in the **a**-axis direction and thus the structure contracts in the **c**-axis

direction. In general, the displacements in the structure result in thermal expansion anisotropy and exhibit a near-zero bulk coefficient of thermal expansion as described by the following equation [12]:

$$\alpha_{bulk} = \frac{1}{3}(2\alpha_a + \alpha_c) \qquad (2\text{-}1)$$

where α_a = average CTE in the a-axis direction,

α_c = average CTE in the c-axis direction.

Some NZP ceramics exhibit thermal expansion hysteresis, in which the expansion curve upon heating differs substantially from the curve upon cooling. The thermal expansion hysteresis is caused by the presence of internal microcracks resulting from thermal expansion anisotropy during processing [13].

Rice et al. [14] and Cleveland et al. [15] observed that the microcracks are dependent on the grain size. No microcracks occur in small-grained solids because the residual stresses resulting from thermal expansion are not sufficient to nucleate microcracks; thus, no thermal expansion hysteresis is observed. On the other hand, in large-grained solids, residual stresses cause microcracks, resulting in large thermal expansion hysteresis.

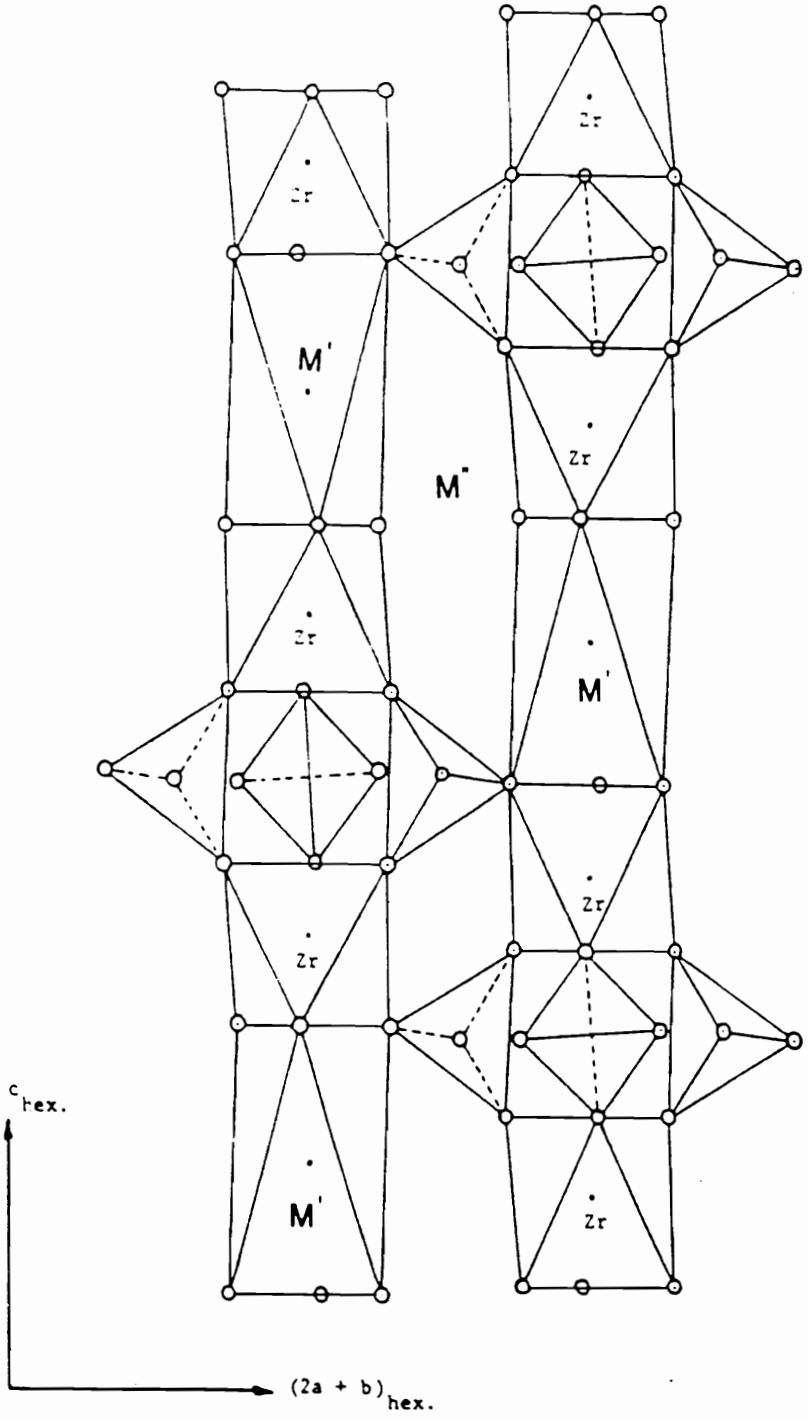

Figure 2.1 Schematic drawing of NZP structure [9]

2.1.2 Thermal Shock Resistance

The resistance of brittle ceramic materials to failure resulting from thermal stress conditions, especially resulting from a rapid change in temperature, is extremely important. The concepts of thermal stress fracture of brittle materials indicate that the resistance of thermal shock damage increases with high values of tensile strength and thermal conductivity, and low values of CTE, Young's modulus, Poisson's ratio, and emissivity. In addition to these factors, Becher et al. [16] found that the thermal shock resistance of a material is increased as the dimensions of the material are decreased. The resistance to thermal shock of ceramic materials can be presented as [17]:

$$\Delta T = \frac{S_t(1-\nu)}{E\alpha} \times \frac{k}{0.31 r_m h} \tag{2-2}$$

where S_t = Tensile strength (psi),

α = Coefficient of thermal expansion (/°C),

ν = Poisson's ratio,

E = Young's modulus (GPa),

k = Thermal conductivity,

r_m = Half thickness of sample (cm),

h = Surface heat transfer coefficient (cal/sec/cm^2/°C).

Hasselman [18,19] proposed that crack propagation under thermal stress conditions generally occurs in the absence of external forces. The driving force for crack propagation rises from the stress field due to thermal expansion anisotropy within the thermally shocked material. Microcracked materials usually exhibit high thermal shock resistance, which is attributed to lower values of Young's modulus and modulus of fracture [18]. NZP ceramics exhibit very good thermal shock resistance because they have near zero bulk thermal expansion and low crystal anisotropy [20, 21].

2.1.3 Flexural Strength

Mechanical behavior, especially strength of NZP ceramics, exhibits a complex dependence on the microstructure and preparation process [20, 21]. The crystalline thermal expansion anisotropy of the NZP structure may produce microcracks in the ceramics which results in low strength.

The relation of microcracking to grain size for polycrystalline ceramics with high thermal expansion anisotropy was reported by Cleveland et al. [15]:

$$G_{cr} = 1.44 r_f / (E \Delta \alpha^2{}_{\max} \Delta T^2) \qquad (2\text{-}3)$$

where G_{cr} is the critical grain size at which microcracking occurs, r_f is the fracture surface energy, E is the single crystal elastic modulus, and α_{max} is the maximum difference in single-crystal thermal expansion coefficients. Another expression can be written as

$$G_{tr} \propto \Delta\alpha^2{}_{\max} \qquad (2\text{-}4)$$

where G_{tr} is the transition grain size at which the ceramic changes from the relatively sound fine grain size region to the microcracked large grain size region.

By applying the above equations, the transition grain size of NZP ceramics can be estimated. When the grain size of NZP ceramics is smaller than the transition grain size, microcracks do not form. In addition, the fine-grained ceramics possess higher strength.

Many processing factors such as sintering temperature, time, and additive, etc., effectively control grain growth of NZP ceramics. Yanai [22] found that the grain growth of NZP ceramics may be suppressed by using additives. Many oxides are effective for this suppression, such as MnO_2, SiO, TiO_2, and V_2O_5.

2.1.4. Corrosion Resistance

Very few papers were found in the literature which deal with the corrosion resistance of NZP ceramics. Li et al. [23] developed CMZP as a member of the NZP family and found that CMZP materials have near zero bulk thermal expansion and low crystal anisotropy, very low thermal conductivity, thermal stability up to 1500°C, excellent thermal shock resistance, and good corrosion resistance to alkali attack [20, 24, 25].

2.2 Aluminum Titanate

2.2.1 Thermal Expansion Behavior

Aluminum titanate is a member of the mixed oxide titanate family of ceramics. There are two allotropic forms of pure aluminum titanate: α-phase, the high-temperature form, which is stable from 1820°C to the melting point of 1860°C, and β-Al_2TiO_5, the low-temperature form, which is stable from room temperature to 750°C and from 1300° C to 1820°C [26]. The β-Al_2TiO_5 is unstable from 750 C to 1300 C, where it decomposes to α-alumina (corundum) and titanate (rutile). The α-phase is not retainable at room temperature, even with rapid quenching [26].

β-aluminum titanate has a face-centered orthorhombic crystal structure with the lattice parameters $\mathbf{a}_0$ = 3.5875A, $\mathbf{b}_0$ = 9.4237A, and $\mathbf{c}_0$ = 9.6291A at 20°C [27].

Since β-aluminum titanate decomposes between 750°C and 1300°C, it needs to be stabilized. The stabilization can be achieved by substituting different cations into its lattice structure. Many stabilizers are available, including rare earth oxides of lanthanum, cerium, and yttrium, as well as SnO_2, MgO, Fe_2O_3, ZrO_2, and Cr_2O_3. As expected, however, these stabilizers alter not only the lattice constants and thermal expansion anisotropy of β-aluminum titanate, but also a number of other physical and mechanical characteristics, including thermal expansion and strength.

Bayer observed that octahedral distortion in the **a**-direction would be reduced and that the smallest lattice parameter, $\mathbf{a}_o$, would become larger if the difference between the ionic radii of the metal ion, Me^{3+}, and Ti^{4+} were smaller [27]. The large distortion in the octahedral of aluminum titanate results in three considerably different lattice thermal expansion coefficients; the thermal expansion coefficients for a single crystal aluminum titanate over a temperature range of 20 - 520°C are $\alpha_a = -3x10^{-6}/°C$, $\alpha_b = 11.8x10^{-6}/°C$, and $\alpha_c = 21x10^{-6}/°C$ [26].

Polycrystalline ceramics are known to spontaneously microcrack from strains resulting from residual stresses due to thermal expansion anisotropy of phase transformations [28]. Extensive microcracking accounts for actual near-zero bulk thermal expansion of polycrystalline AT-80, which is substantially less than the theoretically calculated mean of the lattice expansion coefficients ($(\alpha\mathbf{a}_o + \alpha\mathbf{b}_o + \alpha\mathbf{c}_o)/3$), approximately $9.2x10^{-6}/°C$. In the case of AT-80, pronounced anisotropy of the lattice expansion coefficients results in both intragranular and intergranular microcracking upon cooling from the sintering temperature.

2.2.2 Thermal Shock Resistance

The thermal shock resistance of AT-80 is excellent (>1000°C) due to its extremely low thermal expansion. The CTE is virtually zero because of the presence of microcracks. Therefore, the thermal shock resistance is proportional to grain size as illustrated in Figure 2.2 [29]. The fine-grained aluminum titanate with a grain size below the critical grain size

results in overall less microcracking and, therefore, has only average thermal shock resistance; a coarse-grained AT-80 with a grain size above the critical grain size will exhibit considerabe microcracking and, therefore, has a much better thermal shock resistance.

2.2.3 Mechanical Strength

Since microcracking is gain-size dependent and deleterious to strength, consequently, the strength of AT-80 is very sensitive to grain size. In most aluminum titanate materials containing microcracks, the strength is low. Aluminum titanate ceramics exhibit maximum bend strengths of 20-30 MPa [29]. It should be noted, however, that while microcracking lowers aluminum titanate's elastic modulus, density, and thermal diffusivity, it increases resistance to crack propagation [15].

2.2.4 Corrosion Resistance

Aluminum titanate is well known as a high temperature, low expansion material, and therefore exhibits good thermal shock resistance. Only one paper found in the literature dealt with the corrosion resistance of aluminum titanate [30]. Kang [31] investigated the effects of high temperature, high pressure, steam-alkali environments on the corrosion resistance of silicon carbide coated with aluminum titanate. The aluminum titanate coatings significantly improved the alkali corrosion resistance of the silicon carbide as compared to the uncoated material.

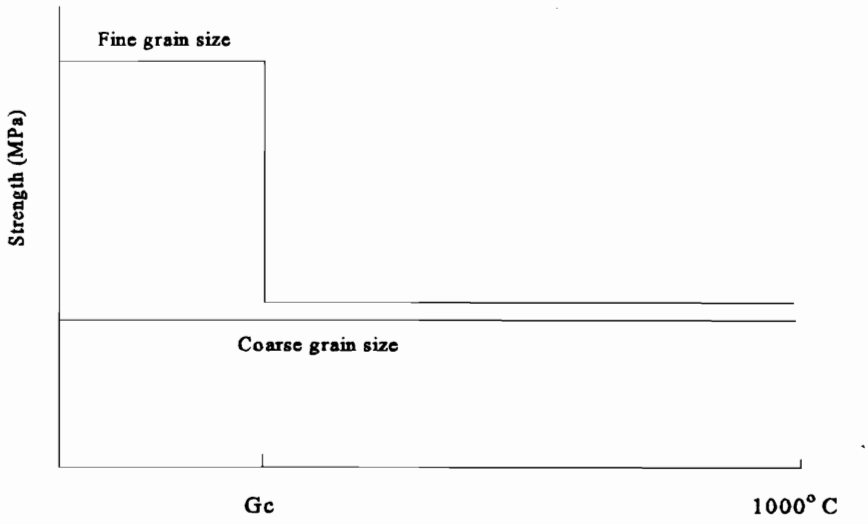

Figure 2.2 The effect of grain size on the thermal shock resistance of aluminum titanate [29].

2.3 Na and V Corrosion

For diesel engine applications sodium salt and vanadia are the main corrosive deposits. Table 2.1 [32] shows the impurities in diesel fuel combustion products at 1050°C for 2 hours. Sodium salt decomposes reacting with some reducing agent to form Na_2O, which interacts with V_2O_5 by the reaction [32]

$$m\ Na_2O + n\ V_2O_5 = m\ Na_2O \cdot (n-p)\ V_2O_5 \cdot p\ V_2O_4 + (1/2)\ p\ O_2 \qquad (2\text{-}5)$$

Such a melt ingresses at the material/oxide interface and evolves oxygen, and as such an oxygen carrier from the atmosphere to the material. However, this reaction depends on the stability of sodium salt and vanadia. For example, the temperature of Na_2CO_3 dissociation is 851°C, so ceramic oxidation with Na_2CO_3 usually is studied at temperatures above 900°C. This is why the oxidation of ceramics in the presence of sodium salt, and vanadia is usually called hot corrosion.

Most oxide ceramics exhibit corrosion resistance to Na and V. For example, stabilized zirconia exhibits good corrosion resistance in diesel fuel combustion products at temperatures up to 850°C. The surface of specimens is not corrosion-damaged. Alumina ceramics are very resistant in an atmosphere simulating the operating environment of gas-turbine engines. These results imply that NZP and aluminum titanate, as oxide ceramics, will likely exhibit good resistance to Na and V corrosion at low temperatures (~700°C).

Table 2.1 Content of impurities of diesel fuel (wt%) [31]

Fuel	Na	V	Ash content
Diesel fuel	$2 * 10^{-9}$	$2 * 10^{-9}$	0.01

Chapter 3. Experimental Procedure

3.1 Materials

The materials used in this study are NZP and aluminum titanate. The compositions of NZP examined were $Ba_{1.25}Zr_4P_{5.5}SiO_{24}$ (BS25) and $Ca_{0.5}Sr_{0.5}Zr_4P_6O_{24}$ (CS50) provided by LoTEC, Inc. A modified stabilized β-aluminum titanate (AT-80) with firing temperatures of 1510°C (AT-80-1510) and 1490°C (AT-80-1490) was provided by GTC.

3.2 Thermal Up Shock

To simulate cast-in-place processing, samples were heated to 1345°C [33] by heating them at 40°C/min, held for 30 min, then air cooled. CTE and modulus of rupture (MOR) were determined before and after up shock. To determine the effect of thermal up shock, CTE and MOR of BS25, CS50, AT-80-1510, and AT-80-1490 were determined before and after up shock.

3.3 Corrosion/Thermal Cycling

After thermal up shock, selected samples were coated with sodium, vanadium, and combined sodium/vanadium solutions to simulate the corrosion environment in diesel engines [34]. The sodium coating used was an aqueous solution containing 6 wt% sodium

nitrate and 24 wt% sodium carbonate. The vanadium solution was formed by mixing 5wt% vanadium oxide in nitric acid. The mixed (Na/V) coating is an aqueous solution of 20wt% sodium vanadate. Samples were coated by dipping into solutions heated to 100°C for 0.5 h, then oven dried at 100°C for 1 h. The coating process was repeated as needed to achieve a coating of approximately 3 mg/cm^2 [32].

To determine the effect of sodium and vanadium on the ceramic under simulated engine conditions, the samples were next cycled from room temperature to 700°C at a rate of 20°C/min, held for 4 h, cooled to room temperature (approximately 2 h), then held for 1 h (Figure 3.1) for 0, 50, and 100 cycles in air. After certain thermal cycling, the samples were washed in boiling water for one hour in order to remove the water soluble corrosion products. The effects of thermal cycling and corrosion were determined by evaluating changes in CTE, weight gain, MOR, and microstructure analysis. Prior to testing, block density was measured using standard ASTM C20-87 method.

3.4 Thermal Expansion

CTE was measured using a Netzsch Dual Push Rod Differential Dilatometer Model-11 with an Al_2O_3 reference. The relative expansion was measured between 30°C and 1000°C with a heating rate of°10 C/min. Measurements were also taken during cooling in order to observe the hysteresis phenomenon. Sample size was 25mm x 4mm x 3mm.

3.5 Flexural Strength

Flexural strength (MOR) was determined at room temperature according to ASTM Standards (C1161-90) using an ATS mechanical testing machine. The inner and outer spans were 20mm and 40mm, respectively. Typically there were 5 test samples for each material. The following equation was used to compute the MOR in MPa:

$$MOR = 3P(L-a)/2wt^2 \qquad (3\text{-}1)$$

where P is the load required to break the bar, and L and a correspond to the lower and upper spans, respectively. The specimen cross section at the break is given by the width w and thickness t.

3.6 Microstructural Analysis

The fracture surfaces from four-point bending specimens before and after thermal up shock, thermal cycling, and combination of corrosion and thermal cycling were examined to determine changes in microstructure of the tested materials. An environmental scanning electron microscope (ESEM) (Electron Scan Corporation Model E-3) was used for the microstructural evaluations.

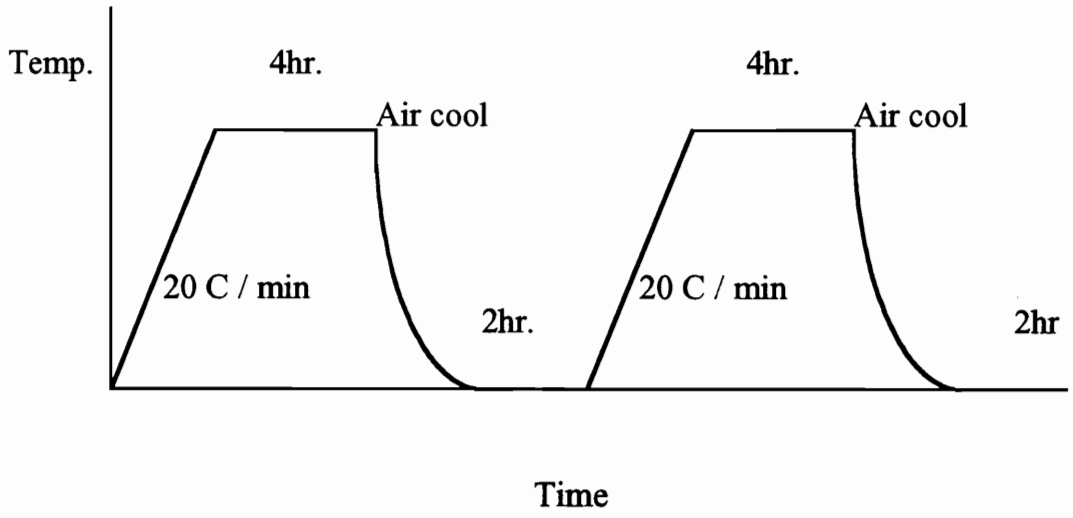

Figure 3.1 Thermal Cycling Regime

3.8 Weight Gain

The weight gain was measured after the samples had been washed for one hour in boiling water in order to remove the corrosion products. If weight gain was less than 0.5 mm/cm^2, it was be assumed to be negligible [32].

Chapter 4. Results and Discussion

4.1 Characterization of As-Received Samples

4.1.1 Thermal Expansion

The relative expansions of NZP ceramics and AT-80 ceramics are shown in Figure 4.1 and Figure 4.2, respectively. Included in the figures are both the heating and cooling portions of the thermal expansion curve. It can be seen that BS25 and CS50 exhibit an isotropic thermal expansion with no thermal expansion hysteresis where the cooling curve lies on top of the heating curve. The AT-80 thermal expansion curve exhibits thermal expansion hysteresis (Figure 4.2). However, all tested ceramics exhibits very low CTE as shown in Table 4.1, which is very important in preventing port liner failure due to thermal shock during the molten metal casting process and for survival under operating conditions.

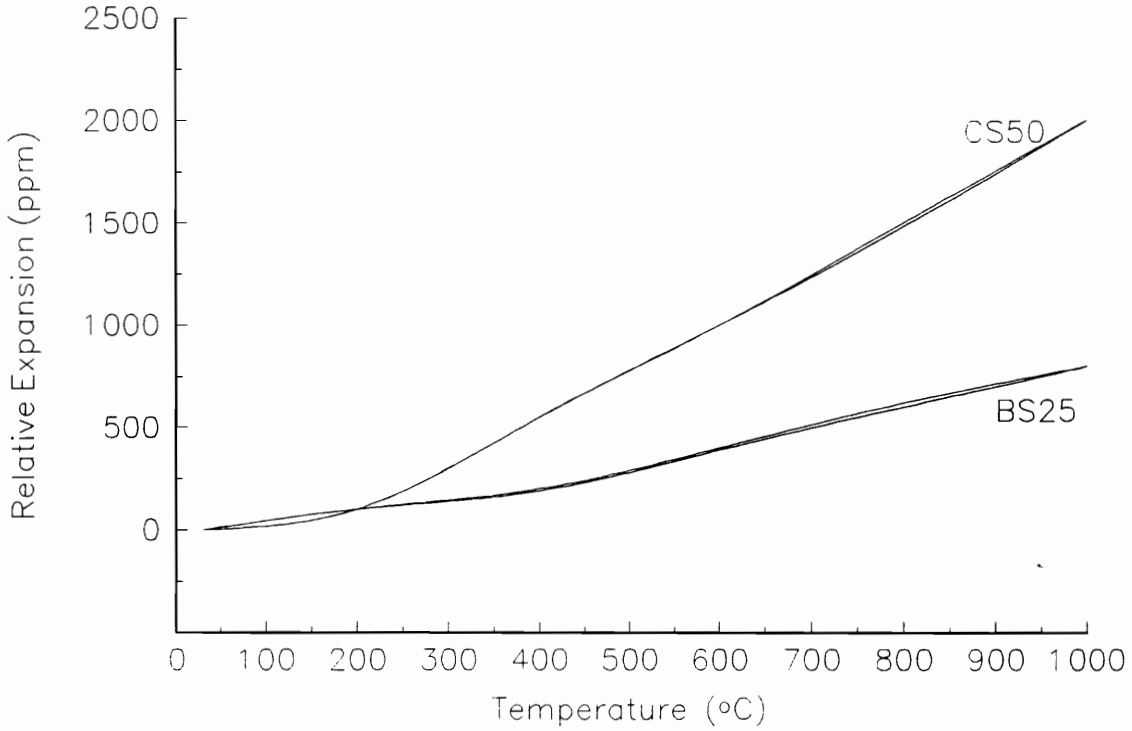

Figure 4.1 Relative expansion of BS25 and CS50 as-received

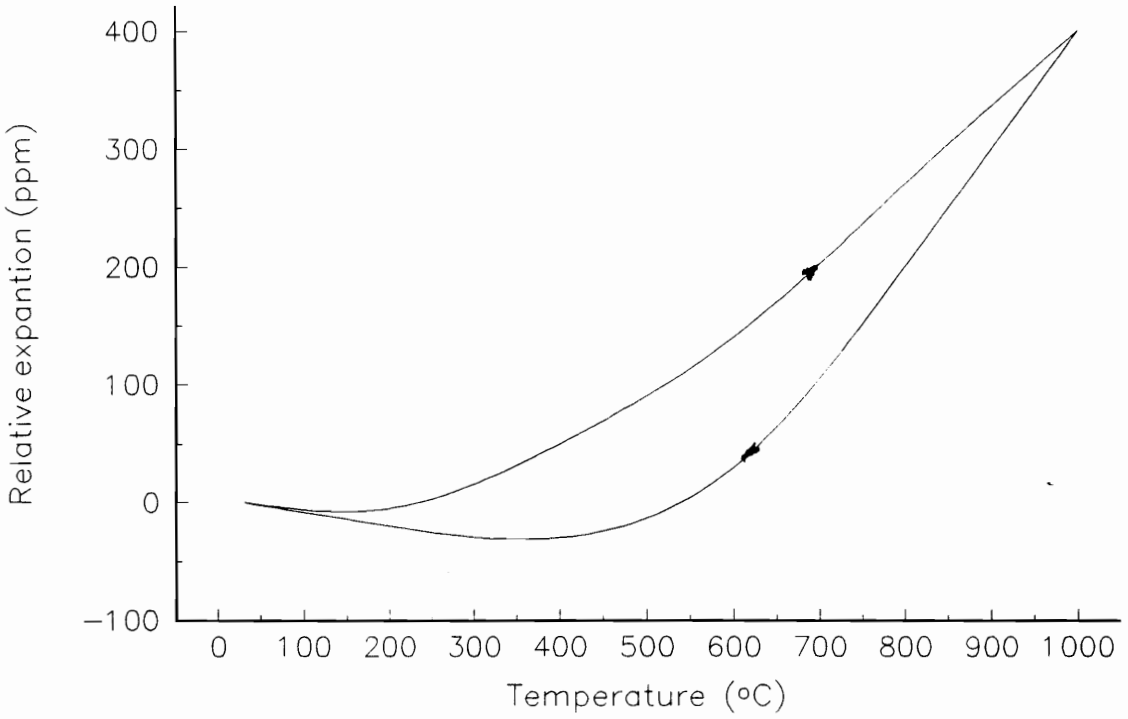

Figure 4.2 Relative expansion of AT-80 as-received

Table 4.1 Properties of NZP and AT-80 ceramics as-received

Material	MOR (MPa)	Density (g/cc)	CTE (10^{-6}/°C)
BS25	86 ±15*	2.9	0.5
CS50	80 ±11	3	1.6
AT-80-1510	24 ±10	3.1	0.5**
At-80-1490	27 ± 8	3.1	0.5**

* Standard Deviation of MOR
** CTE for Specimen AT-80

4.1.2 Flexural Strength

Table 4.1 shows the basic properties of BS25, CS50, AT-80-1510, and AT-80-1490. At room temperature the MOR of BS25, CS50, AT-80-1510, and AT-80-1490 are 86, 80, 24, and 27 MPa, respectively. NZP ceramics exhibited higher flexural strength than aluminum titanate ceramics.

4.1.3 Microstructure

Photomicrographs, Figure 4.3 and Figure 4.4, reveal a similar microstructure for all tested materials, with approximately equal sized grains. However, aluminum titanate ceramics exhibit a larger grain size than NZP ceramics.

The porous structures shown in the photomicrographs reflect the low density of the materials in agreement with that the density for aluminum titanate is 87% of its theoretical value [26] and the density for NZP ceramics is 90% of its theoretical value [33] under the current processing conditions.

For NZP ceramics, CS50 exhibit a slightly larger grain size than BS25, and for aluminum titanate ceramics, AT-80-1510 has a slightly larger grain size than AT-80-1490. The micrographs of the NZP ceramics show transgranular fracture with no microcracks, suggesting that the grains are strongly interconnected (Figure 4.3). However, aluminum titanate ceramics have a significant amount of intergranular fracture with transgranular and intergranular microcracks (Figure 4.4).

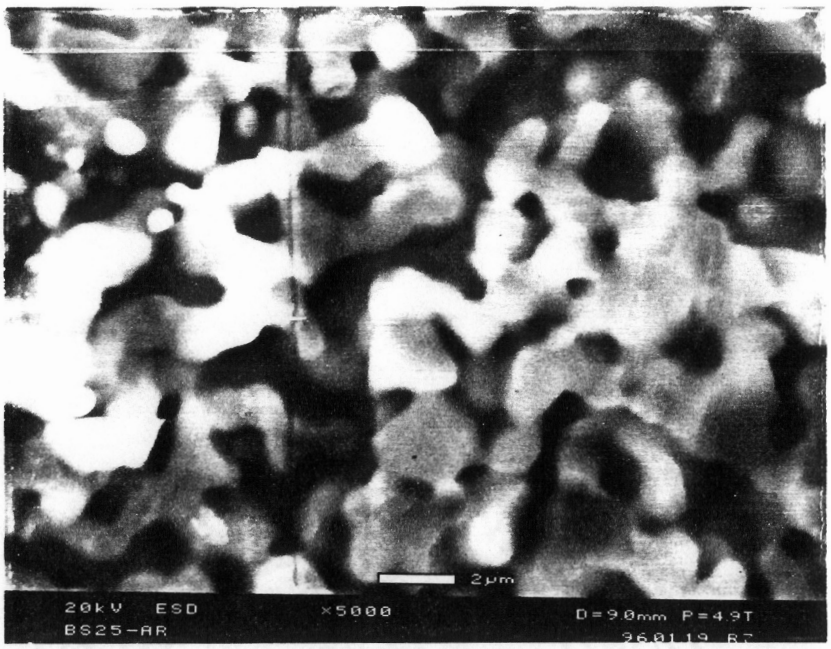

a

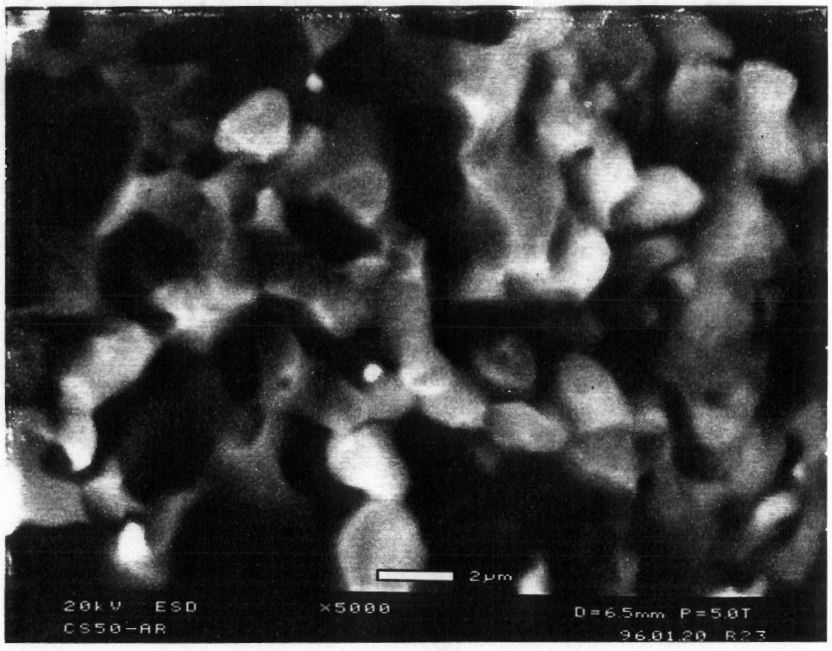

b

Figure 4.3 Microstructure of NZP ceramics as-received

(a) BS25 and (b) CS50.

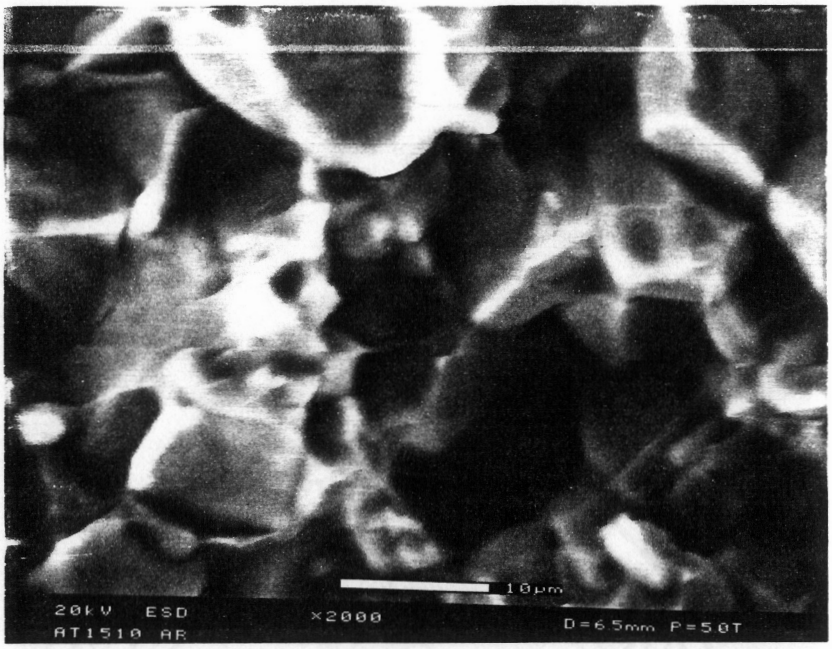

a

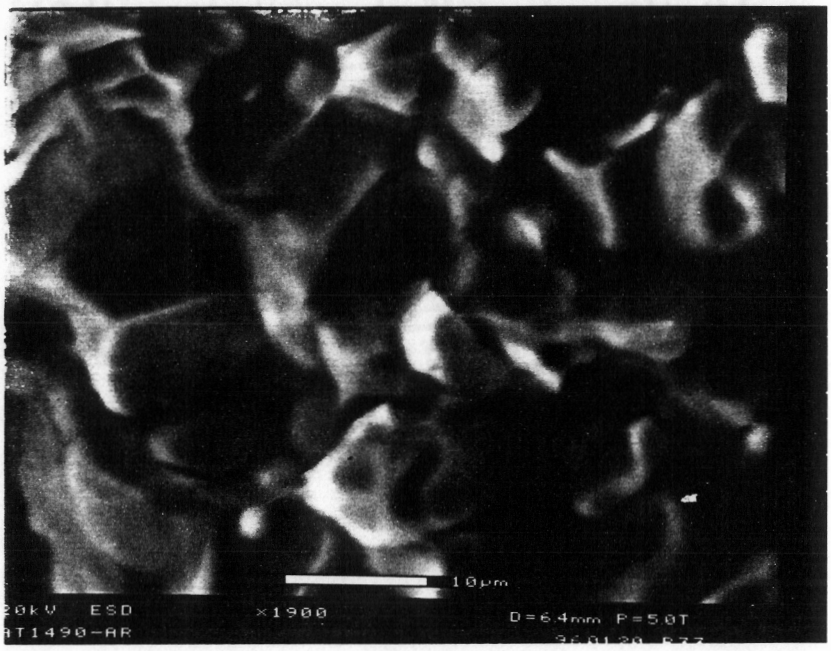

b

Figure 4.4 Microstructure of AT-80 ceramics as-received

(a) AT-80-1510 and (b) At-80-1490

4.2 The Effect of Thermal Up Shock

4.2.1 Thermal Expansion

Thermal expansion was measured for BS25, CS50, and AT-80 after thermal up shock as shown in Figure 4.5. Compared with the as-received samples of BS25, CS50, and AT-80, the CTE of these materials was not significantly affected.

4.2.2 Flexural Strength

Four-point bending tests were completed after the samples had been rapidly heated to 1345°C for 30 minutes then air cooled to room temperature. For BS25, CS50, AT-80-1510, and AT-80-1490, the effect of thermal up shock on MOR was not significant as shown in Table 4.2 and Figure 4.6.

4.2.3 Microstructure

Figure 4.7 and Figure 4.8 show the microstructure of BS25, CS50, AT-80-1510, and AT-80-1490 after up shock. Based on these micrographs, samples subjected to thermal up shock exhibit almost the same microstructure as the as-received samples. No evidence of microcracking or other change was observed in the fracture surface of these materials.

4.2.4 Summary

NZP (BS25 and CS50) and aluminum titanate (AT-80-1590 and AT-80-1490) demonstrate very good resistance to thermal up shock. Exposure to 1345°C at a rapid heating rate did not significantly affect the CTE, MOR, or microstructure of these ceramics.

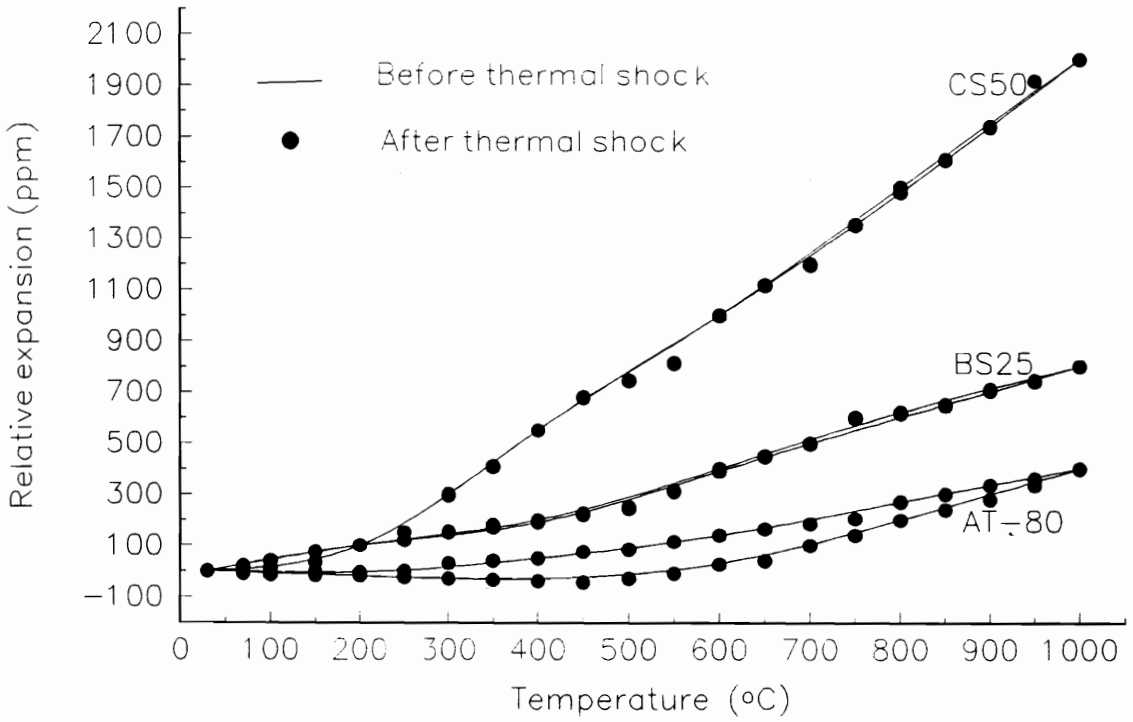

Figure 4.5 Effect of thermal up shock on CTE of NZP and AT-80 ceramics

Table 4.2 MOR of NZP and AT-80 ceramics before and after thermal up shock (MPa).

Condition	BS25	CS50	AT-80-1510	AT-80-1490
As-Received	86±15	80±11	24±10	27± 8
After Thermal Up Shock	79±21	78±13	23±12	26±10

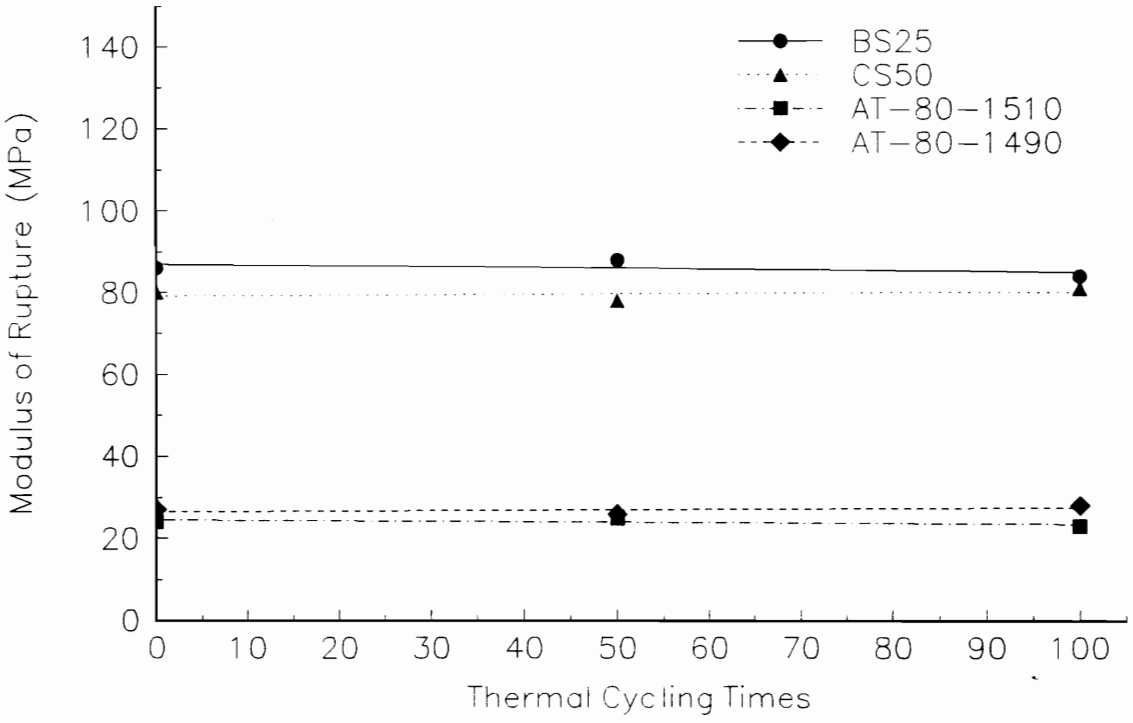

Figure 4.6 MOR of NZP and AT-80 ceramics before and after thermal up shock.

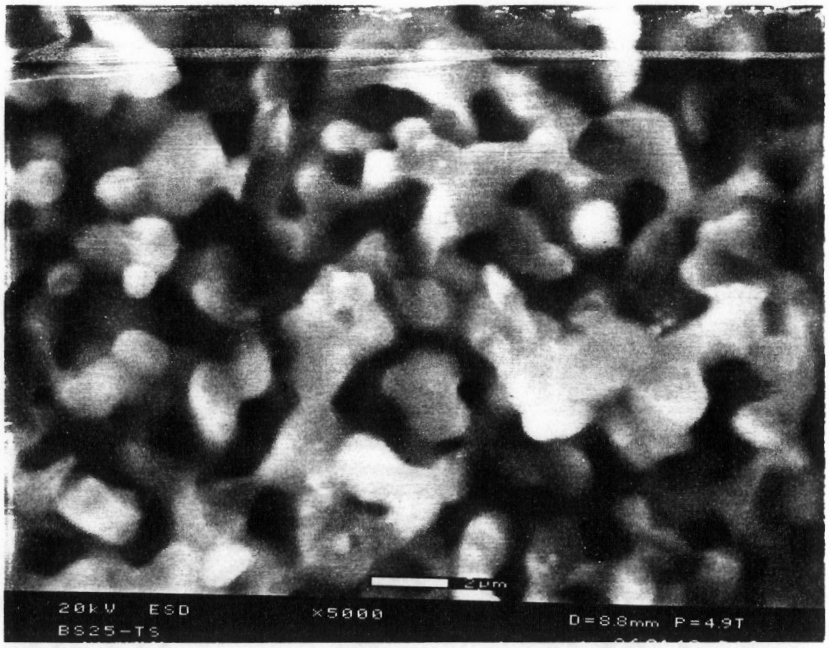

a

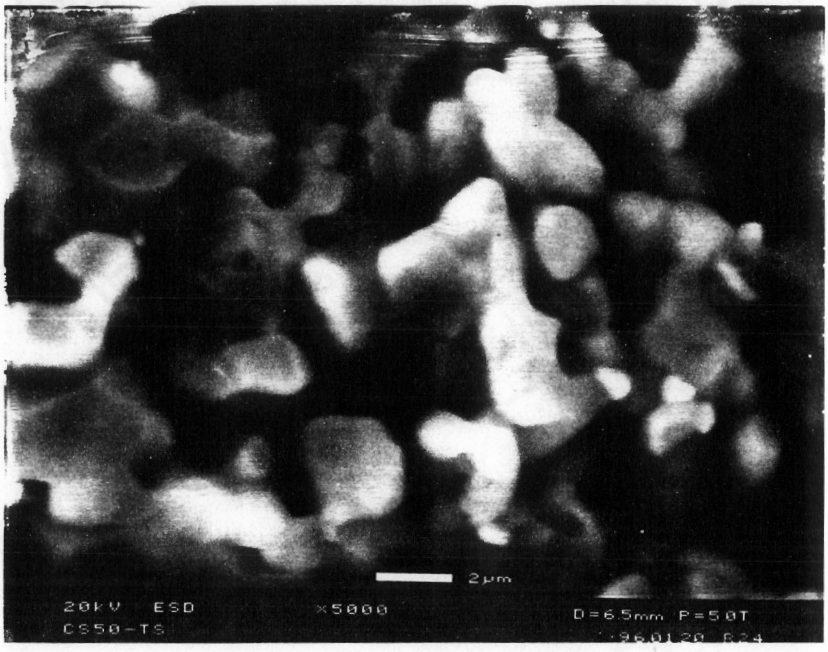

b

Figure 4.7 Microstructure of NZP ceramics after thermal up shock

(a) BS25 and (b) CS50.

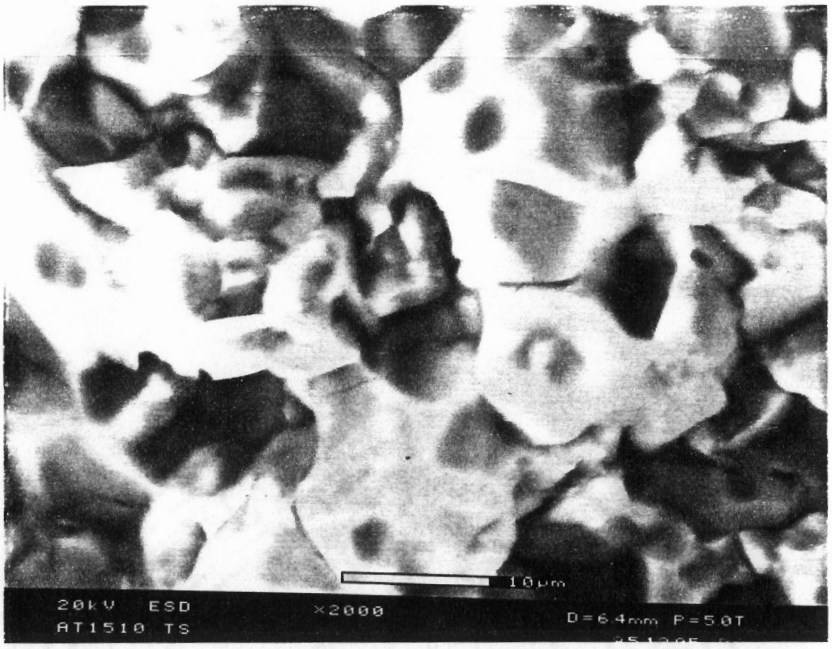

a

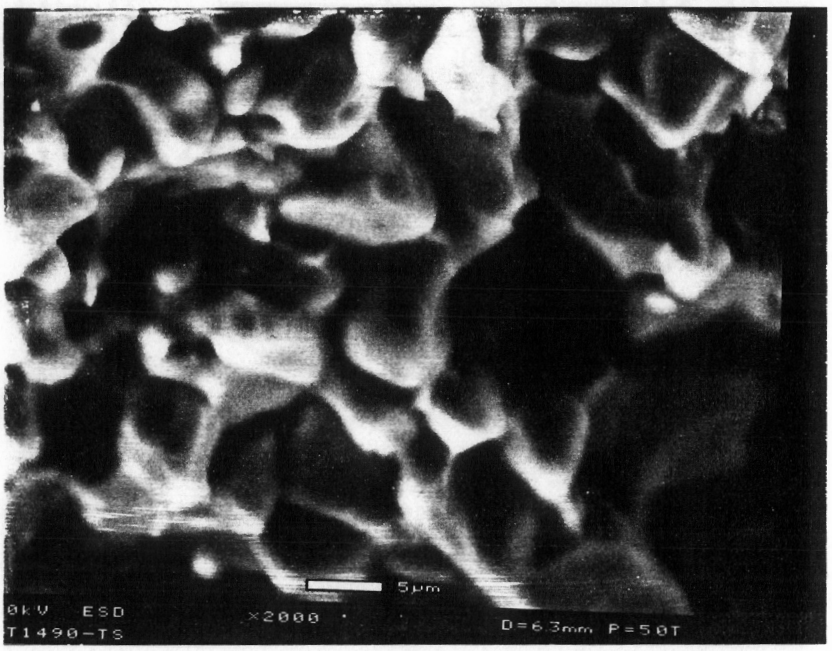

b

Figure 4.8 Microstructure of AT-80 ceramics after thermal up shock

(a) AT-80-1510 and (b) AT-80-1490.

4.3 The Effect of Thermal Cycling

4.3.1 Thermal Expansion

Figures 4.9 and Figure 4.10 show the relative expansions of BS25, CS50, and AT-80. Included in the figures are both the heating and cooling portions of the thermal expansion curve. The CTE curves of all materials tested (BS25, CS50, and AT-80) remains constant after 50 and 100 thermal cycles.

4.3.2 Flexural Strength

The flexural strength of these ceramics is dependent on residual porosity, grain size, number and severity of microcracks, and processing flaws. Porosity and microcracking are the predominant factors. Table 4.3 and Figure 4.11 show that NZP ceramics (BS25 and CS50) exhibit higher MOR than aluminum titanate ceramics (AT-80-1510 and AT-80-1490) after 50 and 100 thermal cycles from room temperature to 700°C. The room temperature flexural strength of these materials was not changed due to crack healing or cracking occurring during thermal cycling. Repeated thermal cycles to 700°C do not have any effect on the flexural strength of these ceramics.

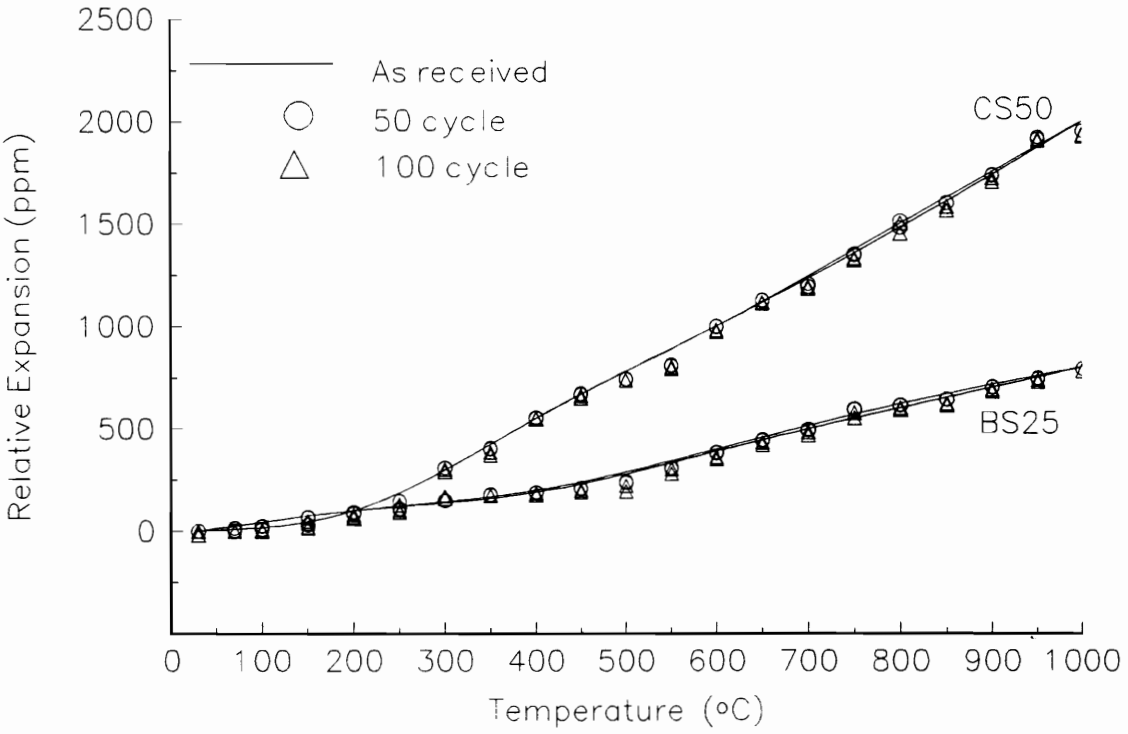

Figure 4.9 Effect of thermal cycling on relative expansion of NZP ceramics

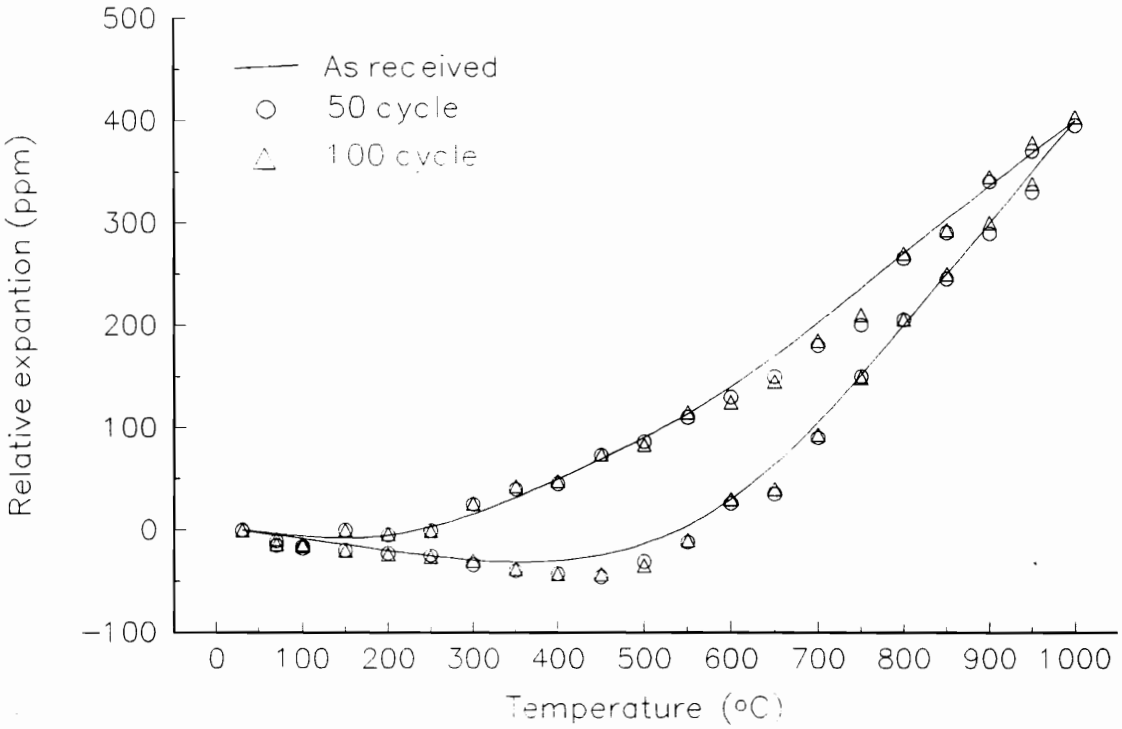

Figure 4.10 Effect of thermal cycling on relative expansion of AT-80

Table 4.3 MOR of NZP and AT-80 ceramics after 50 and 100 Cycles (MPa).

Condition	BS25	CS50	AT-80-1510	AT-80-1490
As-Received	86±15	80±11	24±10	27±8
50 Cycles	88±9	78±12	25±7	26±9
100 Cycles	84±18	81±9	23±9	28±5

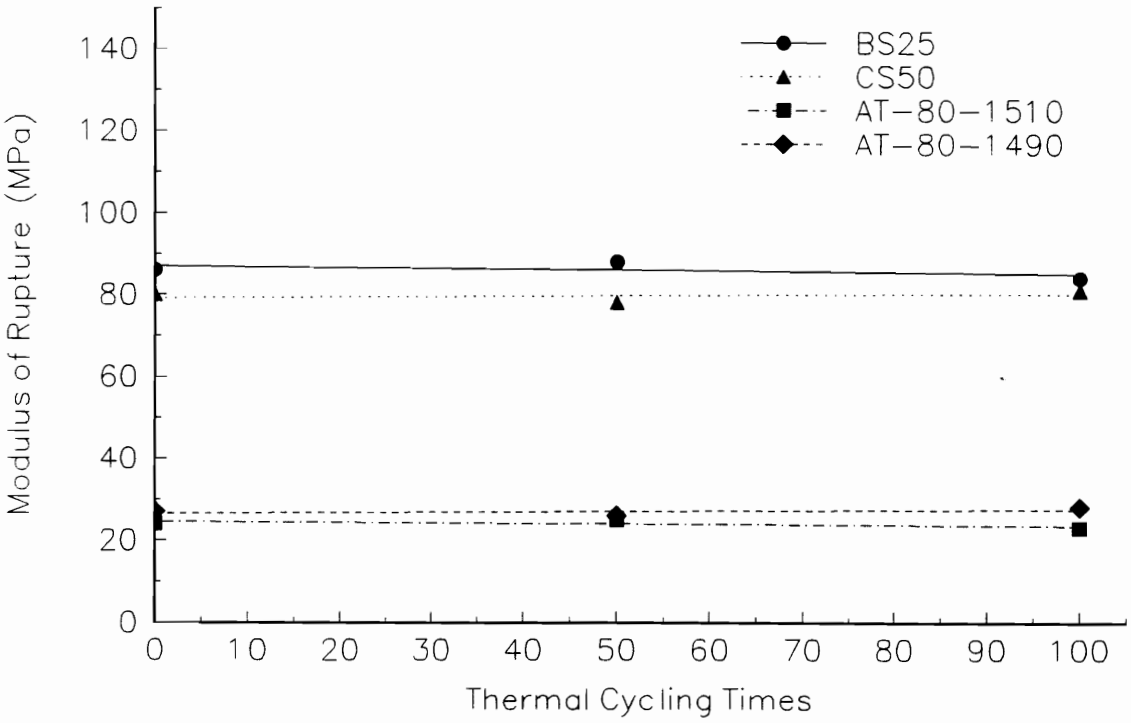

Figure 4.11 MOR of NZP and AT-80 ceramics after thermal cycling.

4.3.3 Microstructure

Figure 4.12 and Figure 4.13 show the microstructure of BS25, CS50, AT-80-1510, and AT-80-1490 after 100 thermal cycles up to 700°C. There is no apparent change in the microstructure. Thermal cycling to 700°C does not affect grain size or microcracking.

4.3.4 Summary

Thermal cycling (from room temperature to 700°C) for up to 100 cycles of NZP (BS25 and CS50) and aluminum titanate (AT-80-1510 and AT-80-1490) has no effect on their thermal and mechanical properties. At temperatures up to 700°C, NZP and aluminum titanate ceramics are very stable.

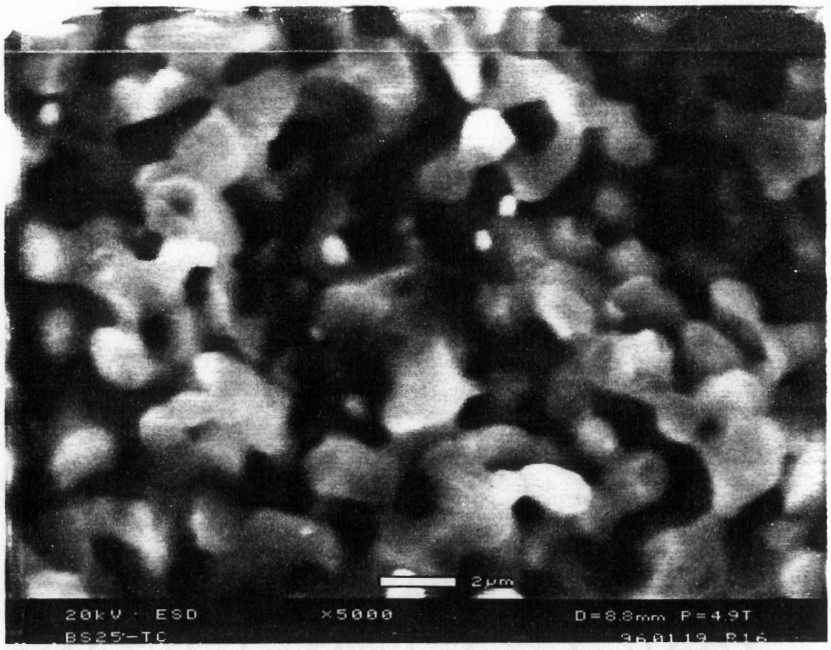

a

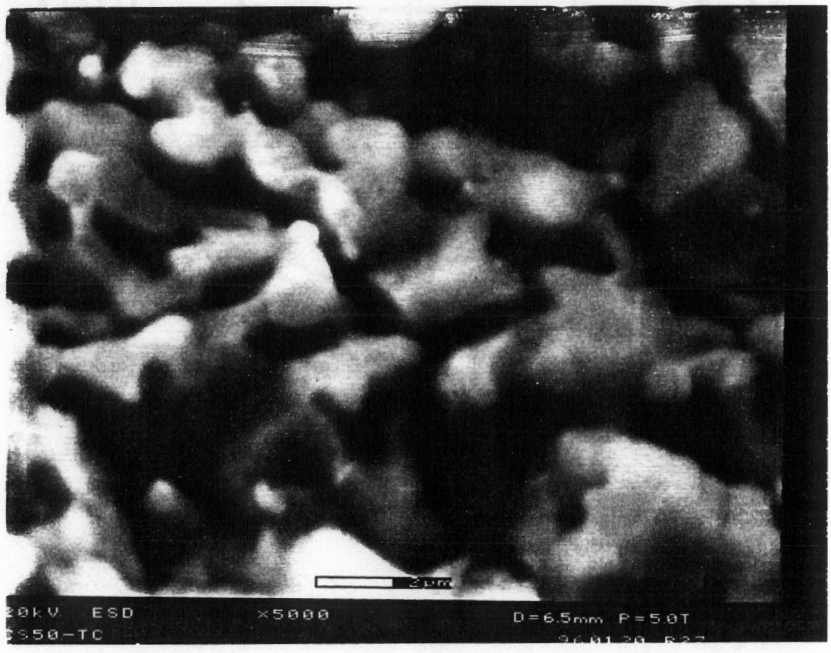

b

Figure 4.12 Microstructure of NZP ceramics after 100 thermal cycles

(a) BS25 and (b) CS50.

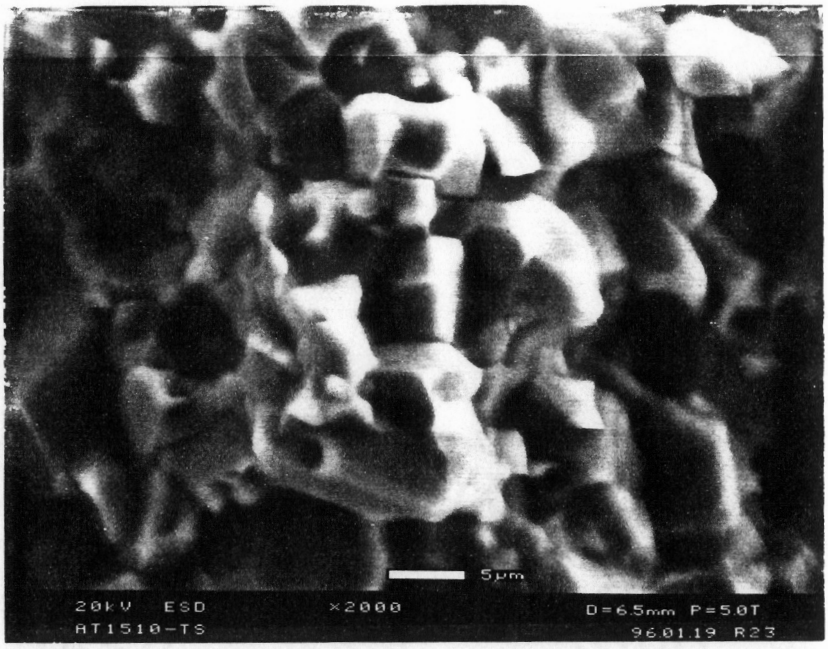

a

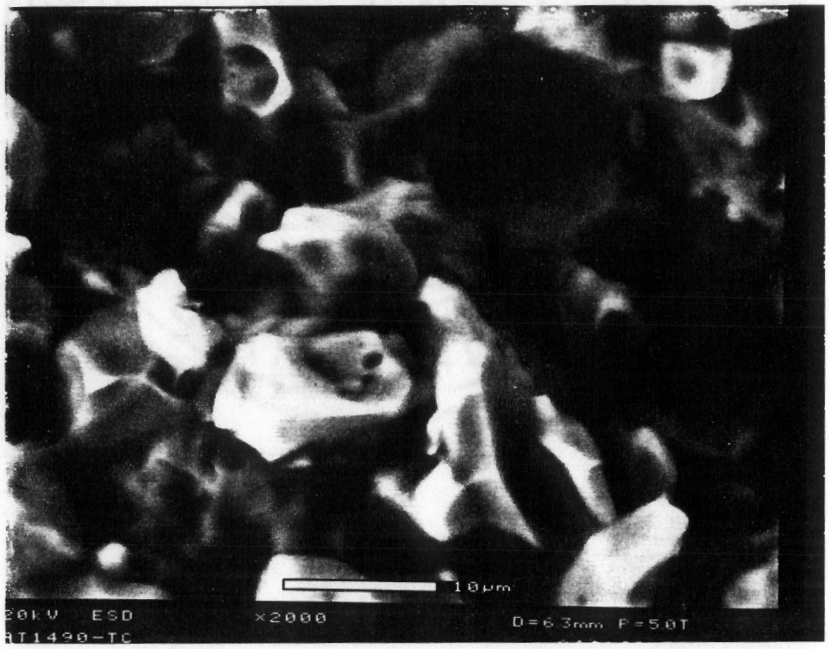

b

Figure 4.13 Microstructure of AT-80 ceramics after 100 thermal cycles

(a) AT-80-1510 and (b) AT-80-1490

4.4 The Effect of Corrosion

4.4.1 Thermal Expansion

Thermal expansion was measured for BS25, CS50, and AT-80 after sodium, vanadium, and sodium/vanadium corrosion with 100 thermal cycles. The combination of corrosion and thermal cycling did not significantly affect these materials as shown in Figure 4.14 and Figure 4.15.

4.4.2 Weight Gain

Table 4.4 shows that the weight gain of NZP and aluminum titanate ceramics for every corrosion condition after 50 and 100 thermal cycles was less than 0.5 mg/cm^2, which indicates that a barrier existed for the transport of the corrosive salt through the corrosion products and the surface of the samples at temperatures up to 700°C. The weight gain for the NZP ceramics in each corrosion condition was slightly higher than that of aluminum titanate ceramics as seen in Figures 4.16, 4.17, and 4.18.

4.4.3 Flexural Strength

MOR of NZP and AT-80 samples after corrosion and 100 thermal cycles are shown in Table 4.5. Figures 4.19, 4.20, and 4.21 show that the MOR of each ceramic is not significantly different from as-received MOR.

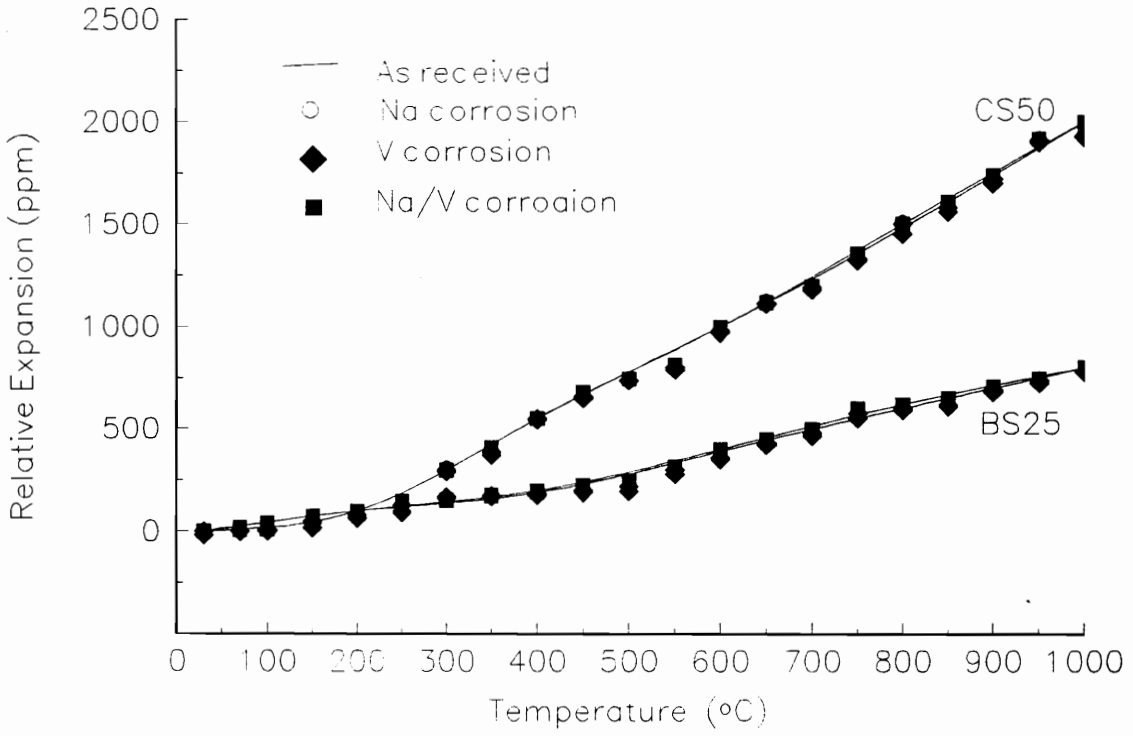

Figure 4.14 Effect of corrosion and thermal cycling on CTE of NZP

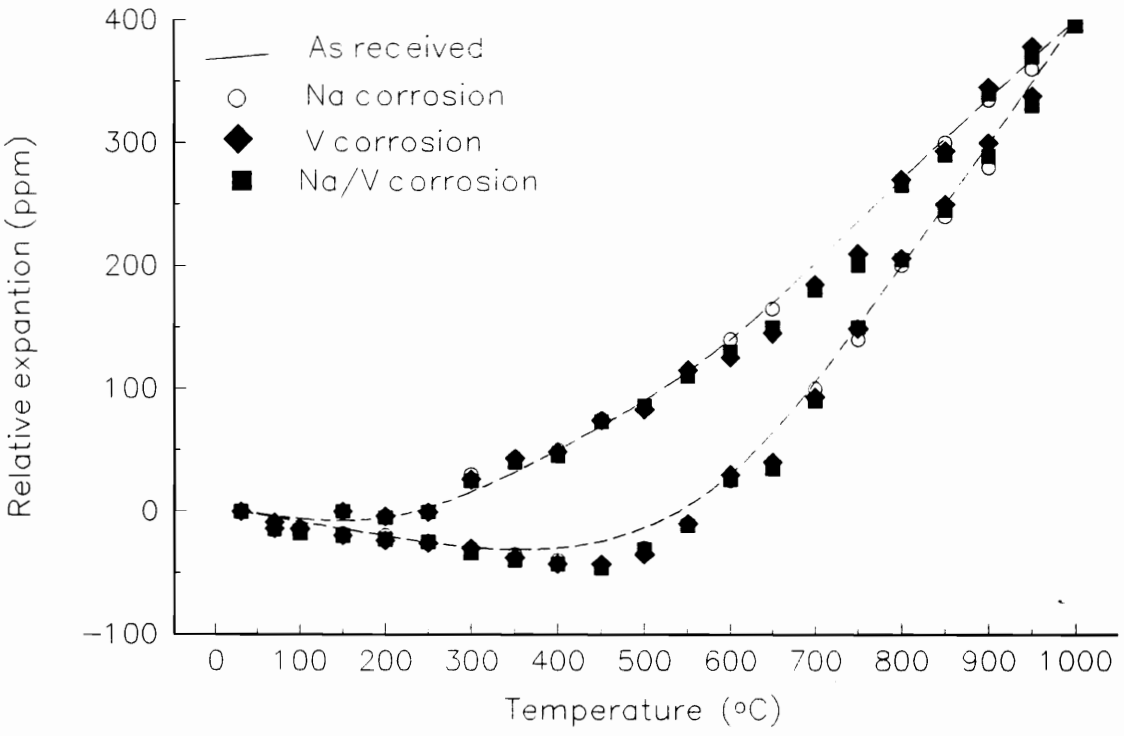

Figure 4.15 Effect of corrosion and thermal cycling on CTE of AT-80

Table 4.4 Weight gain of NZP and AT-80 ceramics after corrosion and 50 and 100 thermal cycles (mg/cm^2).

Corrosion	BS25		CS50		AT-80-1510		AT-80-1490	
	50 cycles	100 cycles	50 cycles	100 cycles	50 cycles	100 cycles	50 cycles	100 cycles
Na	0.16	0.18	0.21	0.2	0.11	0.11	0.09	0.12
V	0.25	0.23	0.11	0.13	0.12	0.10	0.14	0.19
Na/V	0.29	0.34	0.25	0.25	0.16	0.18	0.10	0.15

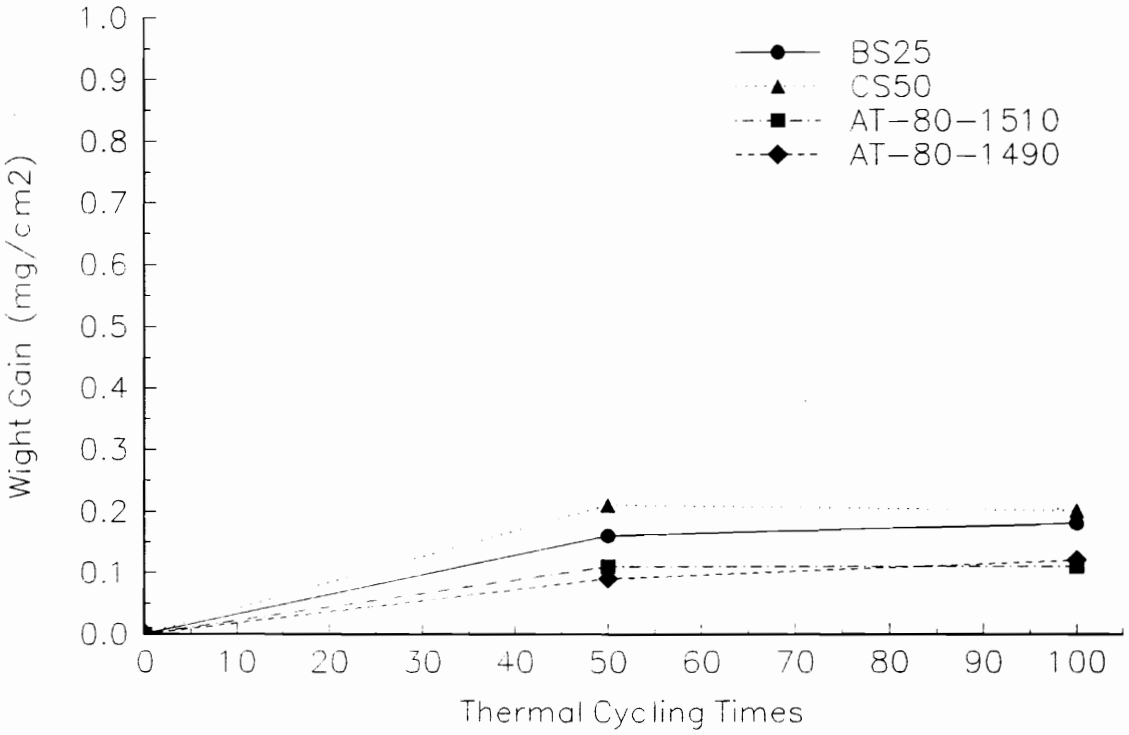

Figure 4.16 Effect of thermal cycling on weight gain after Na corrosion

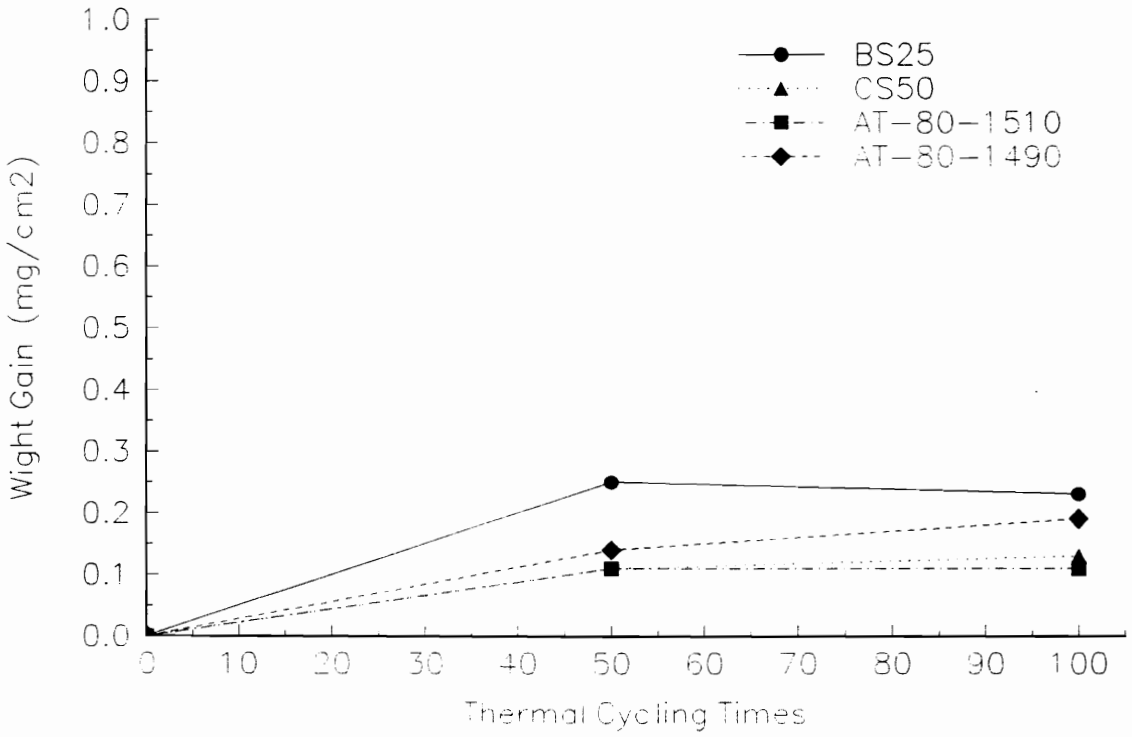

Figure 4.17 Effect of thermal cycling on weight gain after V corrosion

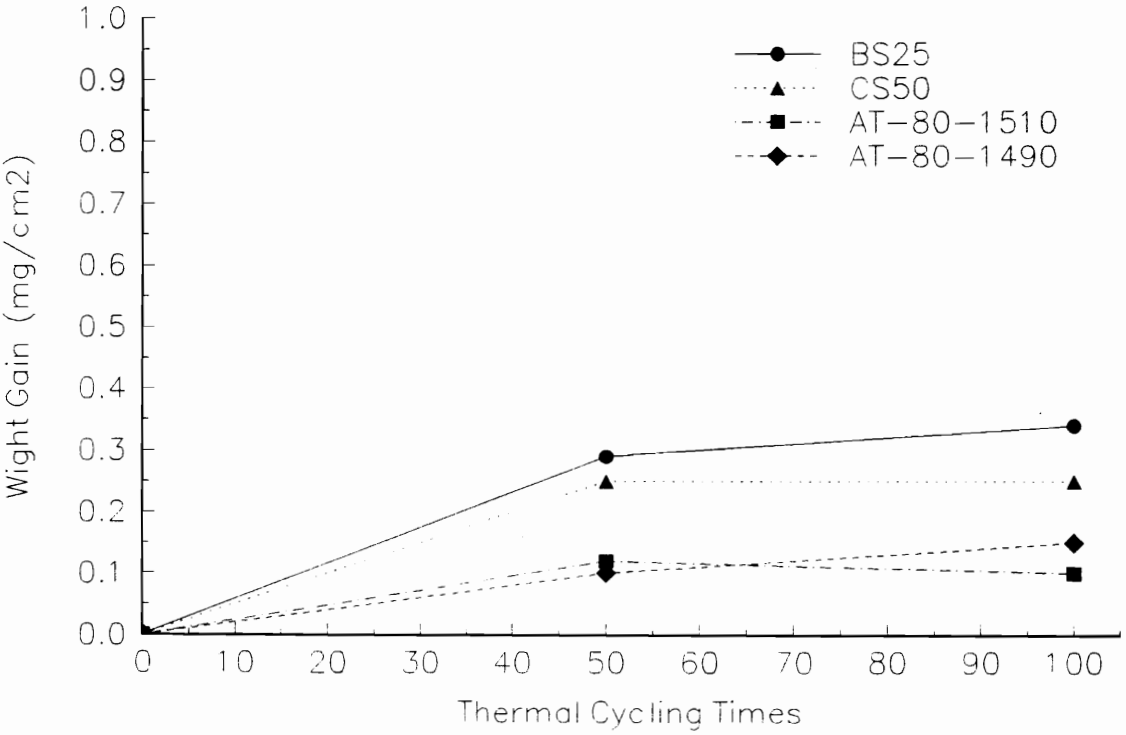

Figure 4.18 Effect of thermal cycling on weight gain after Na/V corrosion

Table 4.5 MOR of NZP and AT-80 ceramics after corrosion and 100 thermal cycles (MPa)

Corrosion	BS25	CS50	AT-80-1510	AT-80-1490
As-received	86±15	80±11	24±10	27±8
100 cycles	84±18	81±9	23±9	28±5
Na	79±20	81±6	23±13	28±3
V	85±10	80±8	24±9	26±10
Na/V	78±19	79±12	22±13	27±3

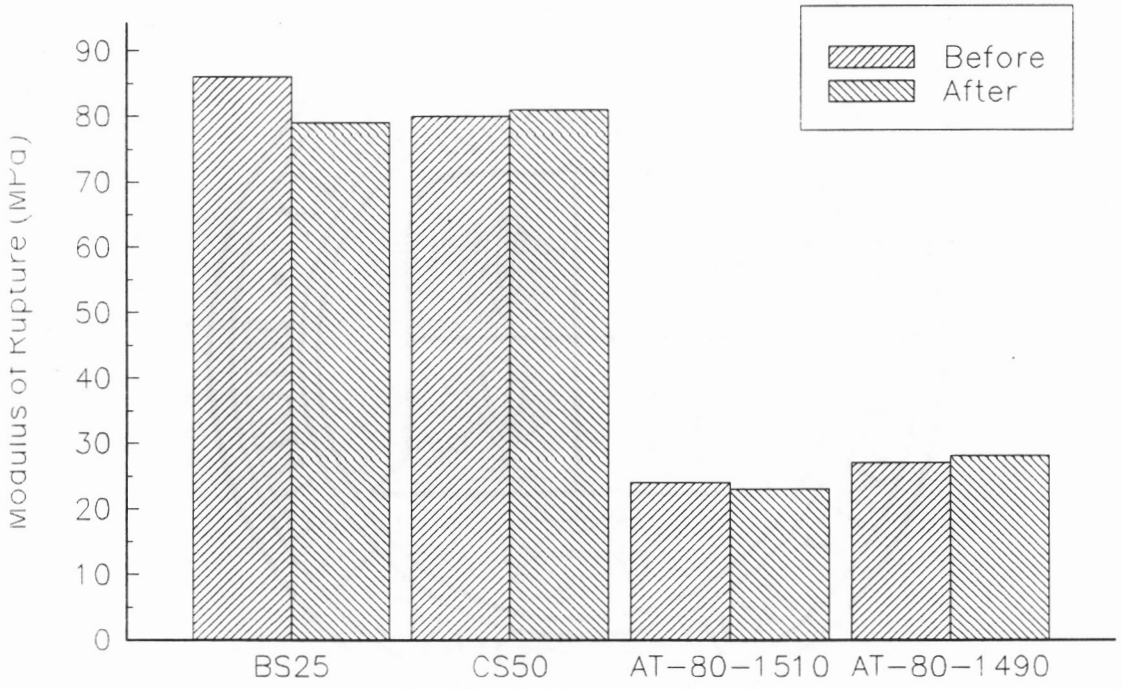

Figure 4.19 Effect of Na corrosion and thermal cycling on MOR of NZP and AT-80

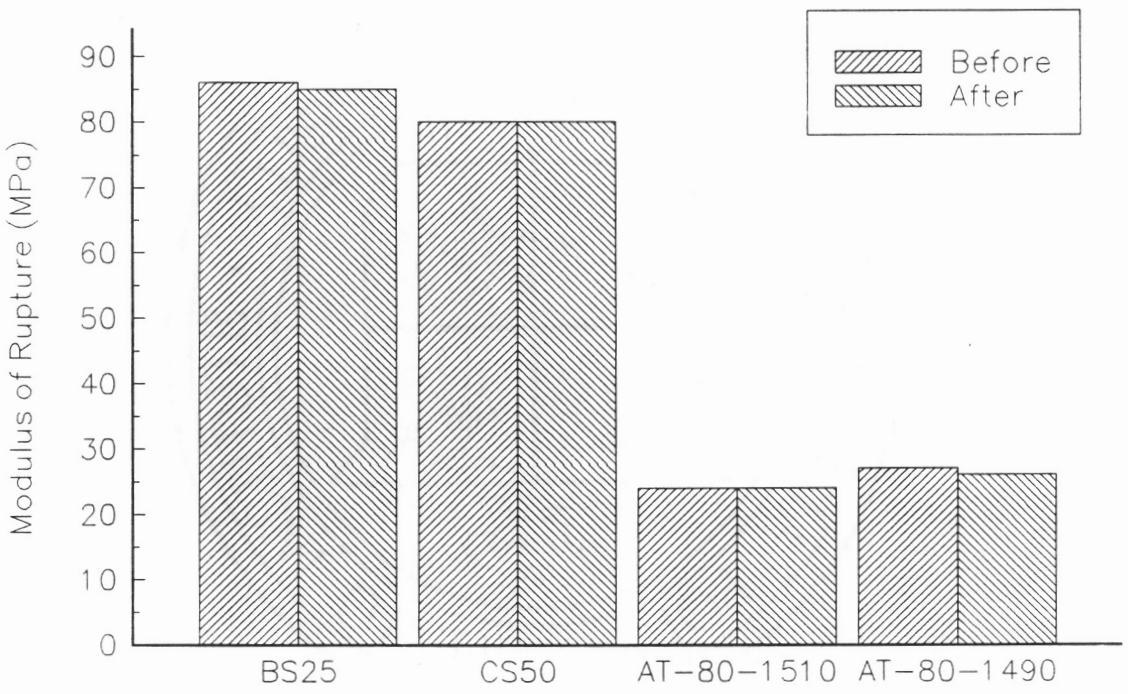

Figure 4.20 Effect of V corrosion and thermal cycling on MOR of NZP and AT-80

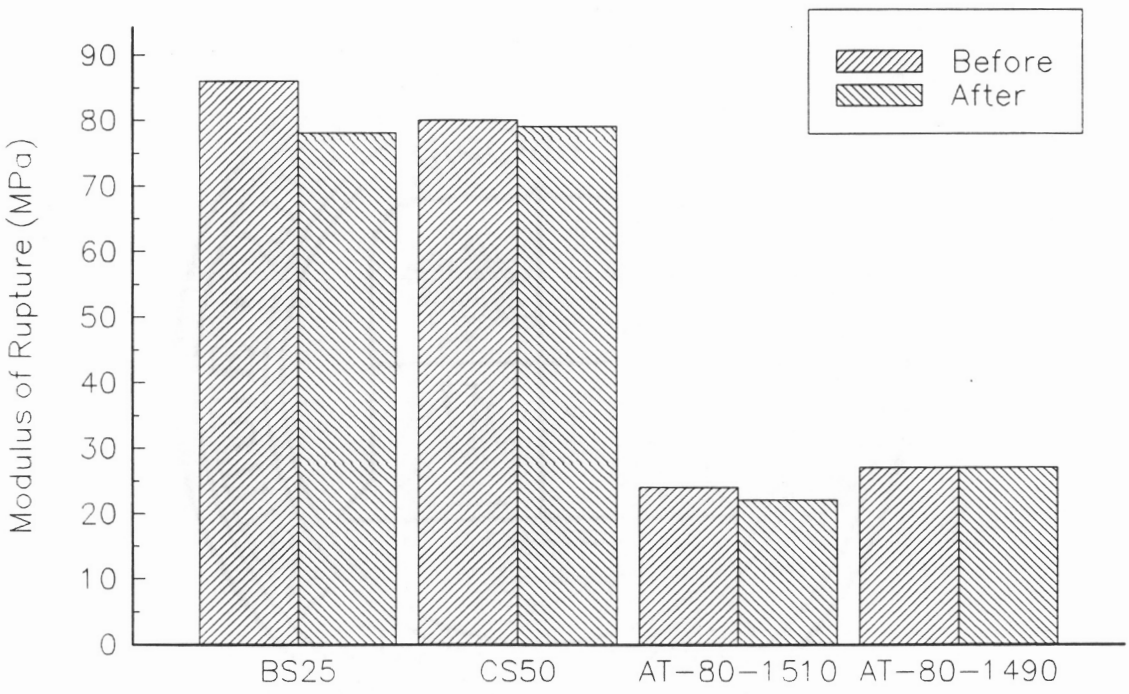

Figure 4.21 Effect of Na/V corrosion and thermal cycling on MOR of NZP and AT-80

4.4.4 Microstructure

Figures 4.22 through 4.25 show the fracture surfaces of BS25, CS50, AT-80-1510, and AT-80-1490 before and after different corrosion tests and 100 thermal cycles. No corroded layer was observed, which indicates no chemical reaction occurred between the ceramics and the corrosion materials. In addition, no internal microstructure change occurred.

4.4.5 Summary

NZP and AT-80 ceramics exhibit good resistance to alkali (Na, V, and Na/V) corrosion combined with thermal cycling.

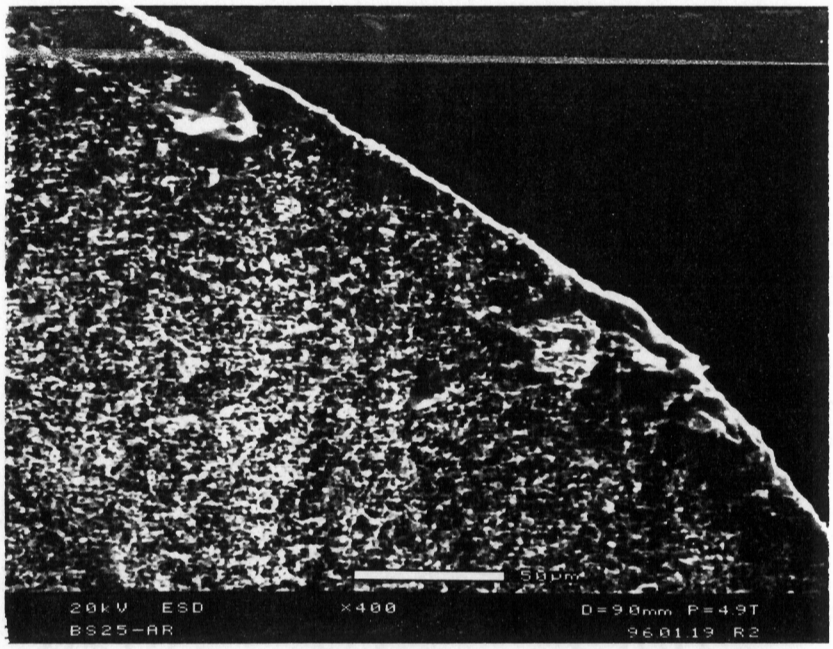

a

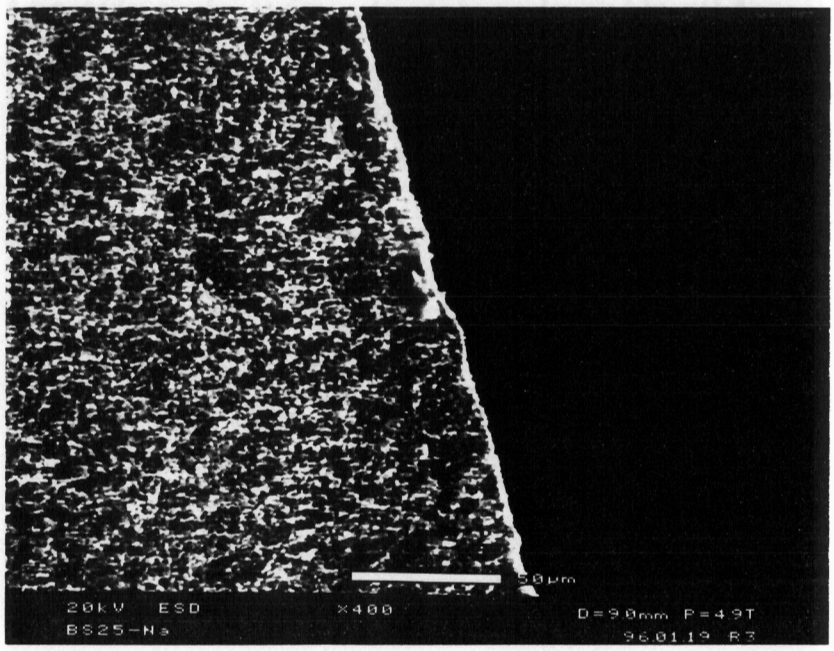

b

Figure 4.22 Microstructure of BS25 after corrosion and thermal cycling.

(a) as-received, and (b) Na corrosion.

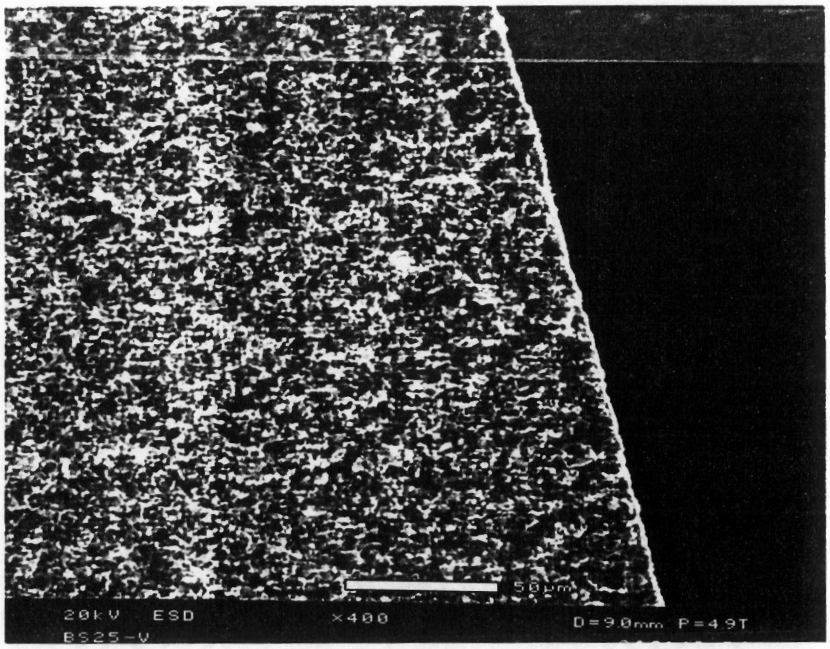

c

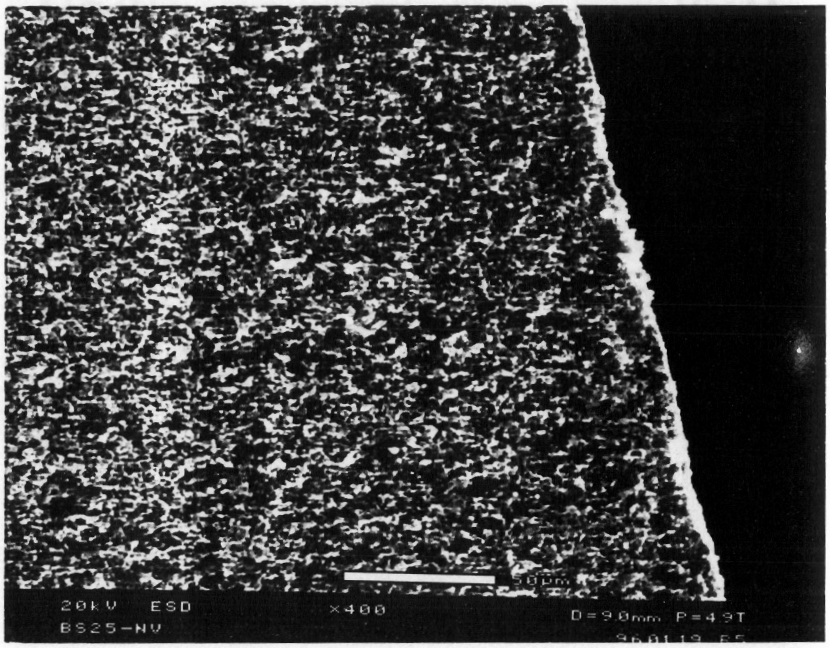

d

Figure 4.22 Microstructure of BS25 after corrosion and thermal cycling

(c) V corrosion and (d) Na/V corrosion.

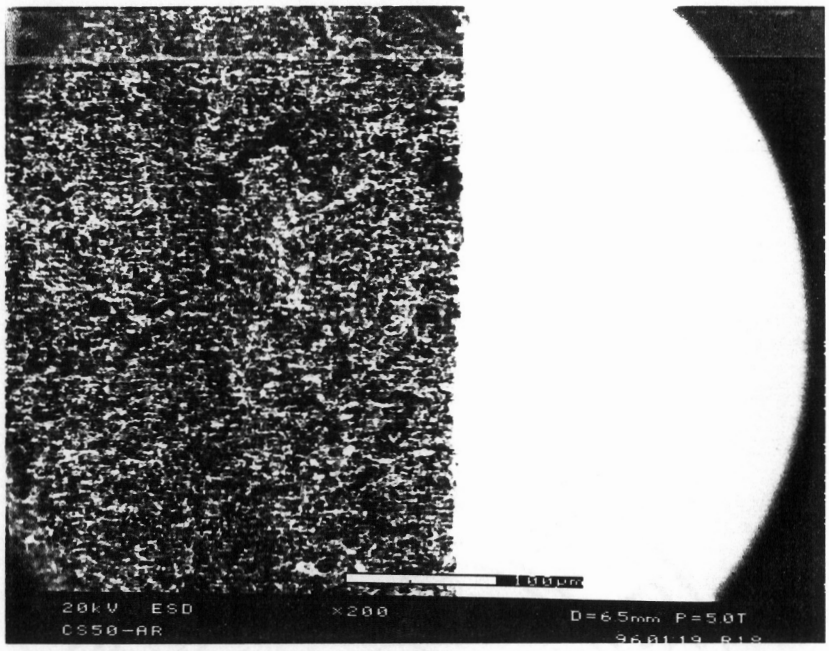

a

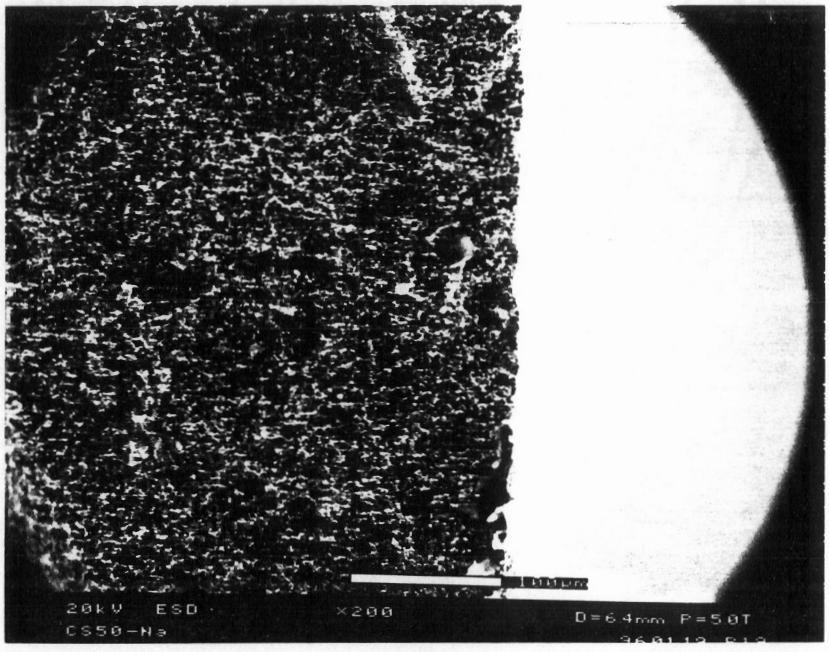

b

Figure 4.23 Microstructure of CS50 after corrosion and thermal cycling

(a) as-received, and (b) Na corrosion

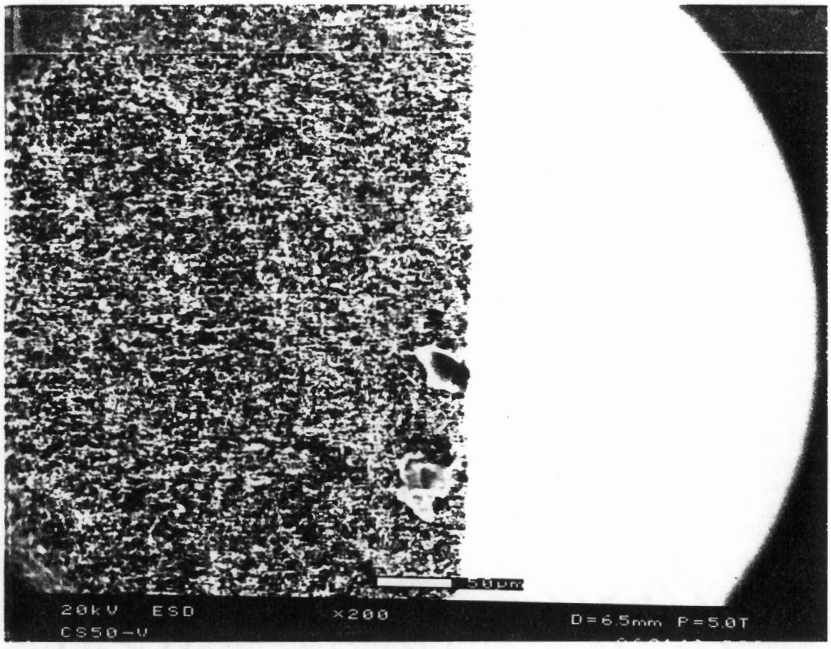

c

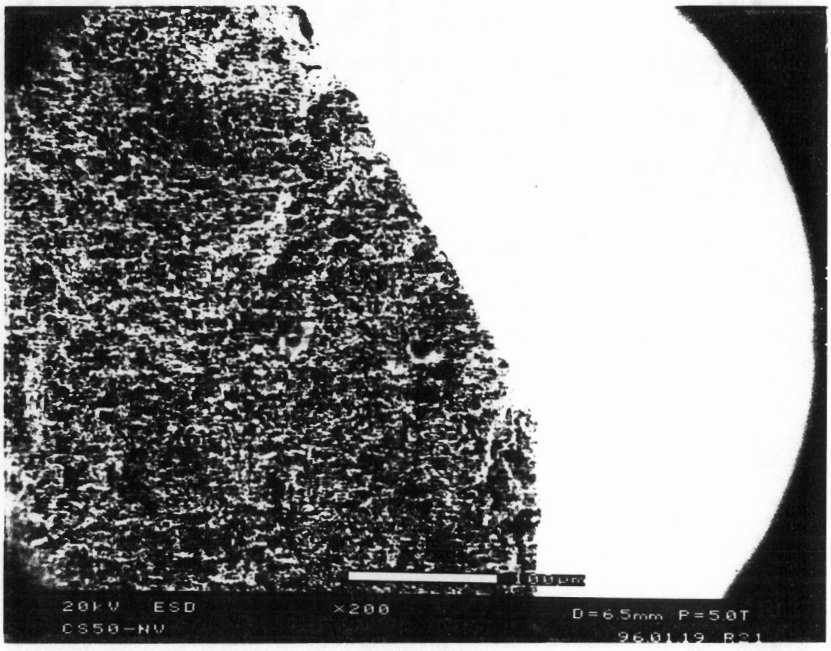

d

Figure 4.23 Microstructure of CS50 after corrosion and thermal cycling

(c) V corrosion and (d) Na/V corrosion.

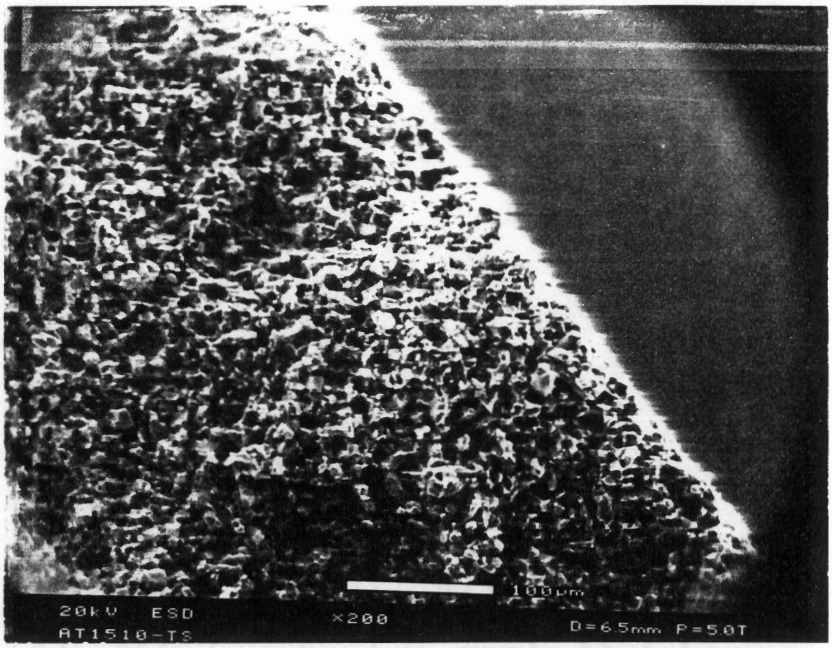

a

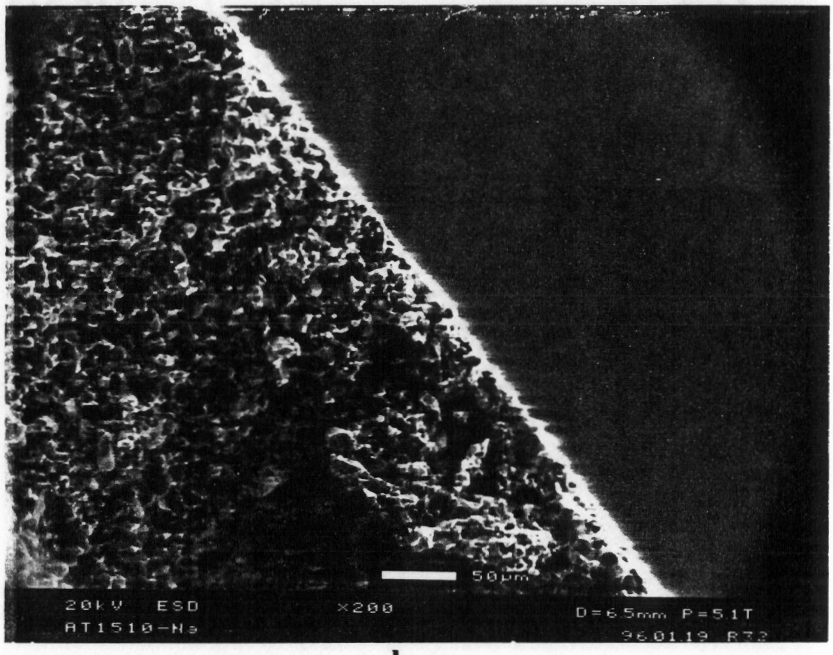

b

Figure 4.24 Microstructure of AT-80-1510 after corrosion and thermal cycling

(a) as-received, and (b) Na corrosion

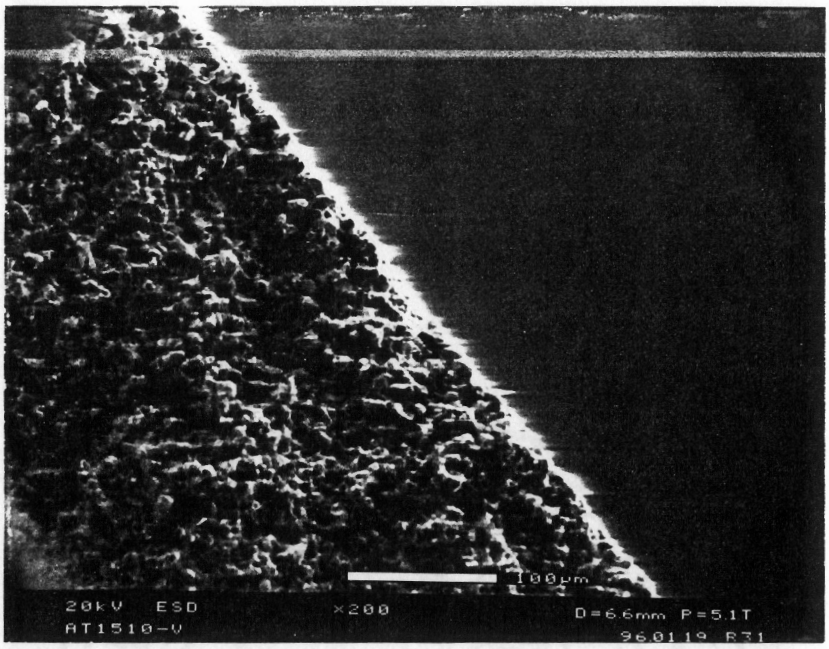

c

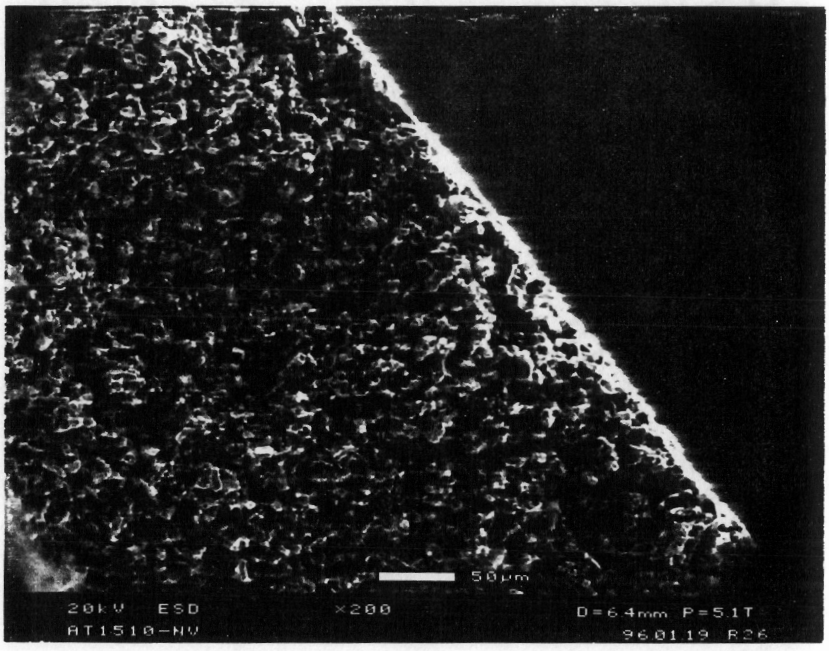

d

Figure 4.24 Microstructure of AT-80-1510 after corrosion and thermal cycling (c) V corrosion and (d) Na/V corrosion.

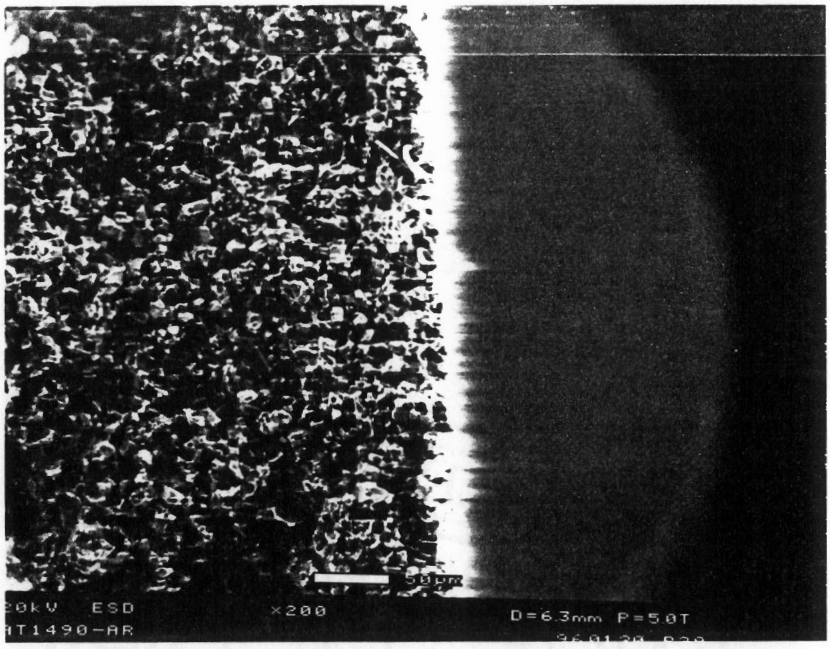

a

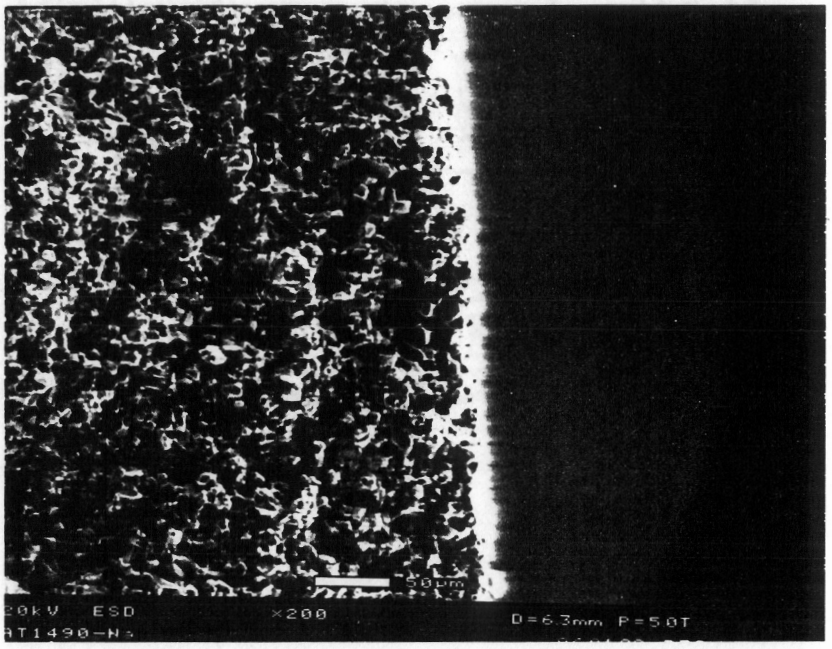

b

Figure 4.25 Microstructure of AT-80-1490 after corrosion and thermal cycling

(a) as-received and (b) Na corrosion.

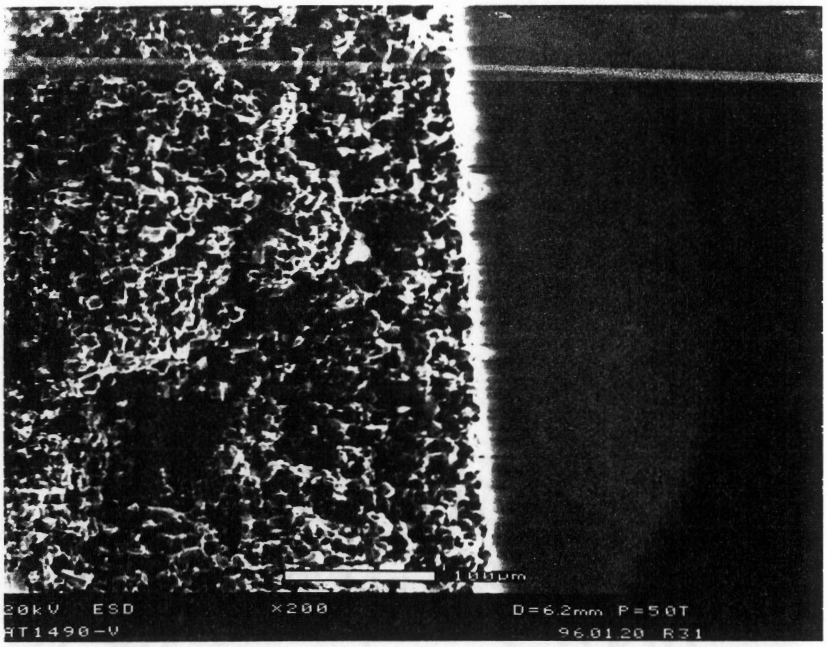

c

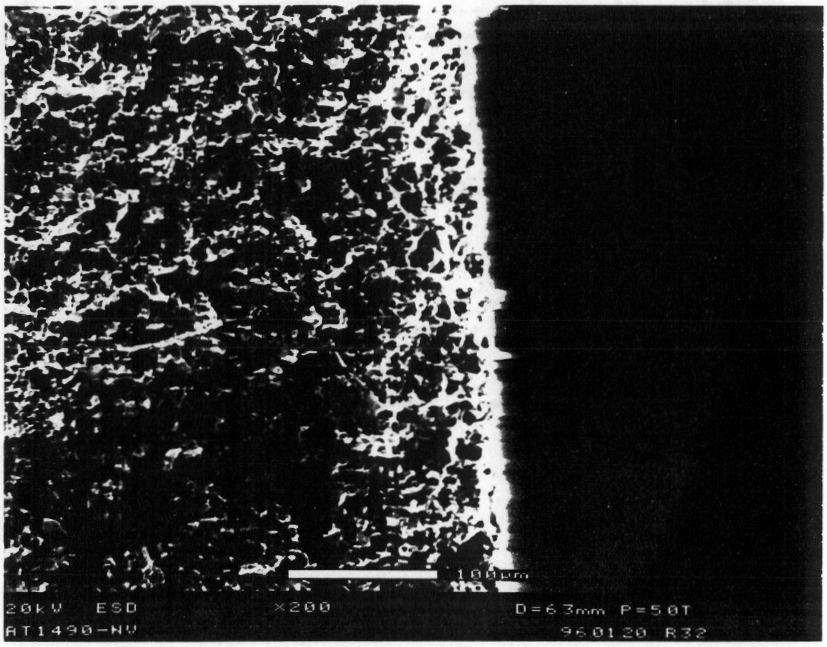

d

Figure 4 25 Microstructure of AT-80-1490 after corrosion and thermal cycling (c) V corrosion and (d) Na/V corrosion.

Chapter 5. Conclusions

5.1 Summary of Results

1. NZP ceramics (BS25 and CS50) exhibit higher flexural strength than aluminum titanate ceramics (AT-80-1510 and AT-80-1490).

2. Both NZP and aluminum titanate ceramics exhibit near zero bulk thermal expansion. NZP (BS25 and CS50) ceramics exhibit isotropic thermal expansion behavior, while aluminum titanate (AT-80) exhibits thermal expansion hysteresis of its microstructure.

3. NZP and aluminum titanate ceramics exhibit good resistance to thermal up shock up to 1345°C due to their low CTE.

4. Thermal cycling to 700°C does not affect thermal expansion or flexural strength of NZP and aluminum titanate ceramics tested.

5. NZP (BS25 and CB50) and aluminum titanate (AT-80-1510 and AT-801490) exhibit good resistance to Na, V, and Na/V corrosion after 100 thermal cycles to 700°C as evidenced by no significant change in weight gain, CTE, and MOR.

5.2 Conclusions

The NZP materials exhibit near zero bulk thermal expansion and isotropic characteristics, thermal up shock resistance, and alkali corrosion resistance in a simulated diesel engine environment, because of their porous structure and low density. Therefore, the NZP ceramics may be suitable for use as cast-in place exhaust port liners and may perform in diesel engine environments. On the other hand, the aluminum titanate materials exhibit aniostropic thermal expansion and lower flexural strength. This is a direct result of the inherent micro-cracking across the aluminum titanate grains upon cooling from the sintering temperature. When AT-80 is employed in applications involving thermal stresses at elevated and fluctuating temperatures as well as alkali corrosion environments, mechanical loading needs to remain minimal.

References

1 R.E. Farris and J.E. Allen, "Albuminous Refractories-Alkali Reactions," *Iron and Steel Engineer*, 2, 67 (1973).

2 M.V. Roode, J.R. Price, et al, "Ceramic Coatings for Corrosion Environments," *Ceram. Eng. Sci. Proc.*, 9 [9-10] 1245 (1988).

3 G.R. Rigby and R. Hutton, "Action of Alkali and Alkali-Vanadium Oxide Slag on Alumina-Silica Refractories," *J. Am. Cerm. Soc.*, 45 [2] 68 (1962).

4 N.S. Jacobson and J. L. Smialek, "Hot Corrosion of Sintered-Sic at 1000°C," *J. Am. Ceram. Soc.*, 68 [8] 432 (1985).

5 J.Sawyer, R.J. Vass, N.R. Brown, and J.J. Brown, "Corrosion and Degradation of Ceramic Particulate Filters in Direct Coal-Fired Turbine Applications," *Trans. ASME, 90-GT-347*, (1991).

6 N.S. Jacobson and D.S. Fox, "Molten-Salt Corrosion of Silicon Nitride: I , Sodium Carbonate," *J. Am. Ceram. Soc.*, 71 [2] 128 (1988).

7 D.S. Fos and N.S. Jacobson, "Molten-Salt Corrosion of Silicon Nitride: II, Sodium Sulfate," *J. Am. Ceram. Soc.*, 71 [2] 139 (1988).

8 H. Hong, "Crystal Structure and Crystal Chemistry in the System $Na_{1+x}Zr_xP_{3-x}O_{12}$," *Mat. Res. Bull.*, 11 173-82 (1976)

9 J. Alamo and R. Roy, "Crystal Chemistry of the $NaZr_2(PO_4)_3$ NZP or CTP, Structure Family," *J. Mat. Sci.*, 21 444-50(1986).

10 L.O. Hagman and P. Kierkegaard, "The Crystal Structure of $NaM_2(PO_4)_3$, M = Ge, Ti, Zr," *XR. Chwm. Scand.*, 22 1822-89 (1986).

11 J.B. Goodenough, H. Hong, and J.A. Kafalas, "Fast Na+---Ion Transport in Skeleton Structures," *Mat. Res. Bull.*, 11 203-06 (1976).

12 S.Y. Limate, et. al., "Synthesis and Thermal Expansion of $MZr_4P_6O_{24}$ (M = Mg, Ca, Sr, Ba)," *J. Am. Ceram. Soc.*, 70 [10]c-232-c-236 (1987).

13 J.A. Kuszky and R.C. Brade, "Influence of Grain Size Effects of Thermal Expansion Anisotropy in $MgTi_2O_5$," *J. Am. Ceram. Soc.*, 56 [8] 420-23 (1973).

14 R.W. Rice and R.C. Pohanka, "Grain-Sized Dependence of Spontaneous Cracking in Ceramics," *J. Am. Ceram. Soc.*, 62 [11-12] 559-63 (1979).

15 J.J. Cleveland and R.C. Brade, "Grain Size/Microcracking Relations for Pseudobrookite Oxides," *J. Am. Ceram. Soc.*, 61 [11-12] 478-81 (1978).

16 P.F. Becher, et al., "Thermal Shock Resistance of Ceramics: Size and Geometry Effects in Quench tests," *Am. Ceram. Soc. Bull.*, 59 [5] 542-48 (1980).

17 W.D. Kingery, "Factors Affecting Thermal Stress Resistance of Ceramic Materials," *J. Am. Ceram. Soc.*, 38 [1] 3-14 (1955).

18 D.P.H. Hasselman, "Unified Theory of Thermal Shock Fracture Initiation and Crack Propagation in Brittle Ceramics," *J. Am. Ceram. Soc.*, 46 [11] 600-04 (1969).

19 D.P.H. Hasselman, "Elastic Energy at Fracture and Surface Energy as Design criteria for Thermal Shock," *J. Am. Ceram. Soc.*, 46 [11] 535-40 (1963).

20 D.A. Hirschfeld. S.M. VanAken, T. Li, Y. Yang and J.J. Brown, "Development of Ultra-Low-Expansion Ceramics: Synthesis, Thermal Expansion, and Thermal Conductivity of $(Ca_{1-x}Mg_x)Zr_4(PO_4)_6$," *Proceedings of the Annual Automotive Technology Development Contractor's Coordination Meeting*, 239, (1990).

21 D.A. Hirschfeld, D. Liu, and J.J. Brown, "CMZP-A New High Temperature Thermal Barrier Material," *4th international Symposium On Ceramic Materials and Components For Engines*, Goteborg, Sweden, June 10-12 (1991).

22 L. Yamai and T. Oota, "Low-Thermal Expansion Polycrystalline Zirconia Phosphate Ceramics: Solid-Solution and Microcracking-Related Properties," *J. Am. Ceram. Soc.*, 68 [5] 273-278 (1985).

23 T. Li, D.A. Hirschfeld, S. VanAken, Y. Yang, and J.J Brown, "The Syntyesis, Sintering, and Thermal Properties of (Ca1-x, Mgx)Zr4(PO)6 (CMZP) Ceramics," *J. Mater. Res.*, 8 [11] 2954-2967 (1993).

24 T. Sun, J.P. Miller, N.R. Brown, and J.J. Brown, "Investigation of Long-Term Thermal/Chemical Degradation of Ceramic Filter Materials," Nov. 1990, *Center for Advanced Ceramic Materials*, Virginia Polytechnic Institute and State University, Blacksburg, VA.

25 D.A. Hirschfeld, Y. Yang, T. Li, and J.J. Brown, "Development of Ultra-Low-Expansion Ceramics: CMZP and CMZP Matrix Composites," *Proceedings of Annual Automotive Technology Development Contractor's Coordination Meeting*, 145-157 (1991).

26 S.M. Lang, C.L. Fillmore, and L.H. Maxwell, "The System Beryllia-Alumina-titanium: Phase Relations and General Physical Properties of Three-Component Porcelains," *J. of Res. of Natl. Bureau of Standards*, 48 [4] 298-312 (1953).

27 C.J. Bayer, "Thermal Expansion Characteristics and Stability of Pseudobrookite-Type Compounds, Me_3O_5," *J. of Less-Common Metals*, 24 129-138 (1971).

28 H.P. Kirchner, and R.M. Gruver, "Strength-Anisotropy-Grain Size Relations in Ceramic Oxides," *J. Am. Ceram. Soc.*, 53 [5] 232-36 (1970).

29 H. Morishima, et al, "Development of Aluminum Titanate -Mullite Composite Having Thermal Shock Resistance," *J. Am. Ceram. Soc.*, 69 [10] c-226-c-227 (1986).

30 J.J. Brown, N. Brown and T. Sun, "Sol-Gel Beta-Aluminum Titanate Thin Film Coating," *Patent Application Filed* 7/93.

31 M. Kang, "Alkali/Steam Corrosion Resistance of Commercial SiC Products Coated with Sol-Gel Deposited Mg-Doped Al_2TiO_5 and CMZP," Master's Thesis, Virginia Polytechnic Institute and State University, 1994.

32 Y.G. Gogotsi and V.A. Lavrenko, "Corrosion of High-Performance Ceramics," pp.61-75, Springer-Verlag, New York, 1992.

33 D. A. Hirschfeld, Personal Communication , May 1995.

34 D. A. Hirschfeld and M. Long, Personal Communication, February 1995.

Vita

The author, Yangsheng Lu, was born on Februray 8, 1960 in She-Yang, Jiangsu, China. She received a B.S. degree in Mechanical Engineering (1982) and a M.S. degree in Metallurgy (1985), both from The Northwestern Polytechnic University (NPU), Xian, China. She worked as a university lecturer and the deputy Director of the Superfine Ceramic Powder Laboratory in the Department of Materials Science and Engineering at the NPU for ten years before she came to the United States. As the first step toward her Ph.D. degree, she joined the Materials Engineering Science doctoral degree program at the Virginia Polytechnic Institute and State University in 1992. The author's optimistic attitude will lead to her ultimate goal as a researcher/educator/leader in materials engineering.

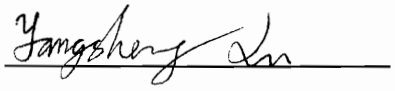

Yangsheng Lu (Signature)